Platinum mineralization in the Kapalagulu Intrusion, western Tanzania

Harry R. Wilhelmij & Louis J. Cabri

Mineralium Deposita
International Journal for Geology, Mineralogy and Geochemistry of Mineral Deposits

ISSN 0026-4598

Miner Deposita
DOI 10.1007/s00126-015-0603-2

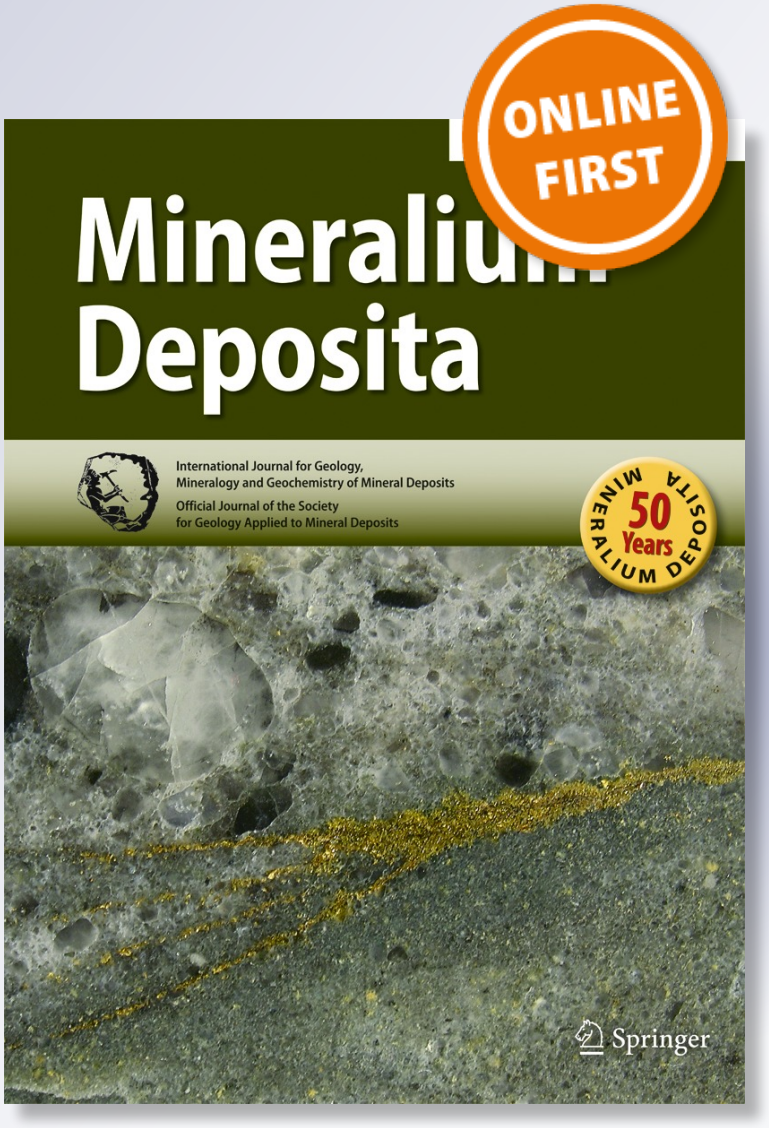

Springer

Miner Deposita
DOI 10.1007/s00126-015-0603-2

ARTICLE

Platinum mineralization in the Kapalagulu Intrusion, western Tanzania

Harry R. Wilhelmij [1,2] · **Louis J. Cabri** [3]

Received: 12 January 2015 / Accepted: 1 July 2015

Abstract Low-grade copper and nickel mineralization was found near the eastern shore of Lake Tanganyika at Kungwe Bay in the early part of the twentieth century. The mineralization occurs in harzburgite at the base of a layered gabbro complex known as the Kapalagulu Intrusion, emplaced between the Paleoproterozoic Ubendian basement and overlying Neoproterozoic Itiaso Group metasediments. Several mining and exploration companies continued the geophysical and drilling exploration for base metals throughout the last century culminating in the discovery of high-grade platinum-group element (PGE) mineralization associated with chromitite and sulfide-bearing harzburgite within the southeastern extension of the Kapalagulu Intrusion (known as the Lubalisi Zone) that is covered by a layer of nickel-rich laterite regolith. The poorly layered southeastern harzburgite forms part of the >1500 m-thick Lower Ultramafic Sequence and resembles a dike-like body that flares upwards into a succession of well-layered gabbroic rocks of the Upper Mafic Sequence. No PGE mineralization has been found in the layered gabbro; all the mineralization is associated with the chromite- and sulfide-rich harzburgite of the Lower Ultramafic Sequence and the laterite regolith overlying the mineralized harzburgite. The Lubalisi Zone harzburgite is underlain by basal dunite and overlain by an interval of layered harzburgite and troctolite and this ultramafic sequence is folded into a syncline that plunges towards the northwest that has been modified by major dolerite-filled faults orientated subparallel to the fold axial surface. Extensive deep drilling in the Lubalisi Zone of the Kapalagulu Intrusion shows that the folded harzburgite can be subdivided into a lower feldspathic harzburgite, a harzburgite containing chromitite seams and intervals of sulfide and chromite mineralization known as the Main Chromite Sulfide Succession (MCSS), an overlying sulfide-rich harzburgite, and an upper feldspathic harzburgite. Impersistent, stratiform PGE mineralized horizons occur within the MCSS harzburgite from which drill core samples were taken for platinum-group mineral (PGM) characterization from two drill holes. Where the PGE reefs reach the surface there is residual PGE mineralization within the laterite regolith from which drill core samples were taken from various laterite lithological units for PGM characterization. As the harzburgite PGE reefs contain significant concentrations of both sulfide and chromite (including chromitite seams) they resemble the PGE-rich chromitite seams of the Bushveld Complex rather than the PGE-bearing Main Sulfide Zone of the Great Dyke and Main Sulfide Layer of the Munni Munni Complex. The dominant Pd PGM in three PGE reef samples varies, ranging (n=164, relative wt%) from bismuthides (63 %), bismuthtellurides (19 %), and tellurides (6 %), to tellurides (39 %), bismuthtellurides (24 %), stannides (14 %), and alloys (13 %), and to antimon-arsenides (33 %), stannides (21 %), bismuthides (17 %), tellurides (13 %), and alloys (10 %). From 13.5 % to 21.0 % of the total Pd occurs as a solid solution in pentlandite. The three samples have similar Pt PGM modal distributions (n=172, relative wt%); the dominant Pt mineral is sperrylite (79, 58, and 47 %) followed by tellurides (15, 17, 21 %), alloys

Editorial handling: W. Maier

Electronic supplementary material The online version of this article (doi:10.1007/s00126-015-0603-2) contains supplementary material, which is available to authorized users.

✉ Louis J. Cabri
lcabri@sympatico.ca

Harry R. Wilhelmij
hwilhelmij@gmail.com

[1] Present address: 3 Norham End, North Oxford, OX2 6SG England, UK

[2] Formerly of Lonmin-Goldstream JV, Perth, Australia

[3] Cabri Consulting Inc., 700-702 Bank Street, PO Box 14087, Ottawa, ON, Canada K1S 3V0

Published online: 03 September 2015

(2, 1, 1 %), and sulfides (2, 1, 0 %). Comparison of Pd/Pt ratios from assays to those calculated from minerals show that the data for the Pt and Pd PGM are very robust, confirming the concentration methodology and characterization. Study of samples from a shallow drill hole penetrating the laterite regolith shows that the primary Pd mineralization has not survived oxidation, is mainly dispersed, but some was reconstituted to form secondary minerals: cabriite, unnamed tellurides, a selenide, a Pd-Te-Hg mineral, alloys and Pd-bearing secondary sulfides (millerite and heazlewoodite). The primary Pt minerals are more resistant to oxidation and dissolution, especially sperrylite and isoferroplatinum, but it is likely that other Pt alloys (tetraferroplatinum and tulameenite) are of secondary origin after dissolution of Pt tellurides.

Keywords Tanzania · Kapalagulu Layered Intrusion · PGM-bearing harzburgite and laterite · Pristine and oxidized PGM quantitative mineralogy

Introduction

Layered gabbroic rocks that form the upper part of the Kapalagulu Intrusion crops out on the side of a mountain range, capped by Neoproterozoic Itiaso Group quartzite, near the eastern shore of Lake Tanganyika at Kungwe Bay. Prospectors in the early part of the twentieth century found low-grade copper and nickel mineralization in a thin basal harzburgite that separates the layered gabbro from gneiss that forms the Paleoproterozoic Ubendian basement. Various mining and exploration companies (INCO, Anglo American, Nippon Mining Company) continued the geophysical and drilling exploration for base metals intermittently during the last century culminating in the discovery by BHP Minerals of platinum mineralization associated with chromitite-bearing harzburgite and nickel-rich laterite that covers the southeastern extension of the Kapalagulu Intrusion.

Van Zyl, while working for INCO in the 1950s, geologically mapped the northwestern exposed portion of the Kapalagulu Intrusion for his MSc thesis (Van Zyl 1956) and outlined the gabbroic stratigraphy of the Upper Mafic Sequence of the Intrusion (Van Zyl 1959; Wadsworth et al. 1982). Almohandis (1984) analyzed chromite concentrations in core samples of basal harzburgite from INCO's diamond drill holes located in the northern part of the Kapalagulu Intrusion and concluded that the chromites have less chromium than those of the Bushveld and Stillwater intrusions. More recent geological research on the Kapalagulu Intrusion included geochemical and mineralogical examination of 31 core samples from the INCO drill holes and rock chip samples (Maier et al. 2007, 2008) collected from the upper part of the Kapalagulu Intrusion by Van Zyl in the 1950s during his field mapping (Van Zyl 1956; 1959). It was concluded that the Kapalagulu magma assimilated about 15 % of sedimentary rocks leading to the enrichment of the magma and cumulates in incompatible trace elements. This assimilation of crustal sulfide resulted in early sulfide saturation of the magma. Maier et al. (2007) also made radiometric age determinations of the Kapalagulu Intrusion (1392±26 Ma) from the same suite of samples collected by Van Zyl.

Boniface collected eclogite and metapelite samples from the Paleoproterozoic Ubendian gneiss to the west of the Kapalagulu Intrusion to identify the metamorphic history for his PhD thesis (Boniface 2009). He concluded that the metamorphic rocks represented oceanic lithosphere that had been subducted and experienced repeated regional metamorphic events following their emplacement into the continental crust (Boniface and Schenk 2012; Boniface et al. 2012).

From 2001 to 2009, Goldstream Mining in Joint Venture with Lonmin PLC explored for platinum and nickel in both the laterite and harzburgite protolith in the southeastern dike-like extension of the Kapalagulu Intrusion known as the Lubalisi Zone. During this period, exploration consisted of airborne and ground geophysical electromagnetic, magnetic and radiometric surveys, grid-based soil sampling, geological mapping and 53,227 m of drilling which included 124 diamond (34,041 m), 729 air core (14,182 m), 213 rotary air blast (4000 m) and 11 reverse circulation (1004 m) drill holes. All of the drill chips and diamond drill core were geologically logged and sampled to determine base and precious-metal content. Samples were also taken from some of the drill core for mineralogical, petrological, and metallurgical investigations. This exploration led to a good understanding of the spatial distribution of the nickel-bearing laterites and underlying ultramafic stratigraphy, and the structure and mineralization of the layered ultramafic rocks. A summary of the exploration results of the earlier part of this program of work were presented by Wilhelmij and Joseph (2004); they described the stratigraphic location of PGE reefs present near the middle of a thick sequence of harzburgite that occupies much of the Lower Ultramafic Sequence present in the Lubalisi Zone, and preliminary PGM mineralogical results.

The goal of the PGM study for the fresh harzburgite samples (four samples from inclined drill holes KPD 24 and 44) was to determine the petrography, nature of the PGM, mineralogical association of platinum-group element (PGE) mineralization, and the mineral liberation characteristics in the four samples, and provide comments on possible mineralogical and processing implications.

The goal of the PGM study for the laterite samples (five samples from inclined drill hole KPD 22) was to identify the stable PGM, to determine what has happened to the Pd minerals and the Pd previously held in solid solution in pentlandite, to determine if any Pt and Pd oxides are present, their abundance, and speciation, and to discuss the mineralogy in terms of its impact on processing and metallurgy, and provide,

if possible, insight on the Ni distribution. The processing and metallurgy parts of the study are discussed in a separate paper (Cabri and Wilhelmij 2015).

The present paper summarizes highlights from these investigations together with a description of the geological setting of the PGM mineralization within both the harzburgite protolith and the overlying laterite in the expectation that this first detailed, but still preliminary, account of the mineralization will lead to more in-depth investigations.

Central African nickel belt

The Kapalagulu Intrusion lies near the eastern shore of Lake Tanganyika in Western Tanzania and forms part of a series of mafic and ultramafic intrusions that include Musongati and Kabanga stretching from northwestern Tanzania across Burundi into western Tanzania. These intrusions are known as the Central African Nickel Belt (Fig. 1, and cf., Duchesne et al. 2004; Maier et al. 2008). There are other less well-known intrusions to the west of Lake Tanganyika in the Democratic Republic of the Congo.

The Central African Nickel Belt intrusions, which have an age of about 1400 Ma, were emplaced into the Mesoproterozoic Kibaran orogenic belt (1100 to 1400 Ma) and the Paleoproterozoic Ubendian basement (older than 1800 Ma). As the Kapalagulu Intrusion has been intruded between the basal unconformity of the folded Itiaso Group metasediments (Kibaran) and the Ubendian basement, the intrusion must be younger than 1400 Ma (Deblond et al. 2001; Maier et al. 2007).

Kapalagulu Intrusion structure and stratigraphy

Parts of the Kapalagulu Intrusion are well exposed along a series of ridges to the east of the small village of Makambo located on Kungwe Bay of eastern Lake Tanganyika. These ridges culminate in an escarpment formed by resistant quartzite and phyllite of the Itiaso Group metasediments that are in faulted contact with gabbro of the Kapalagulu Intrusion. Consequently, the true stratigraphic extent of the upper part of the intrusion is not known. The layered gabbroic rocks that form the ridges represent the Upper Mafic Sequence of the

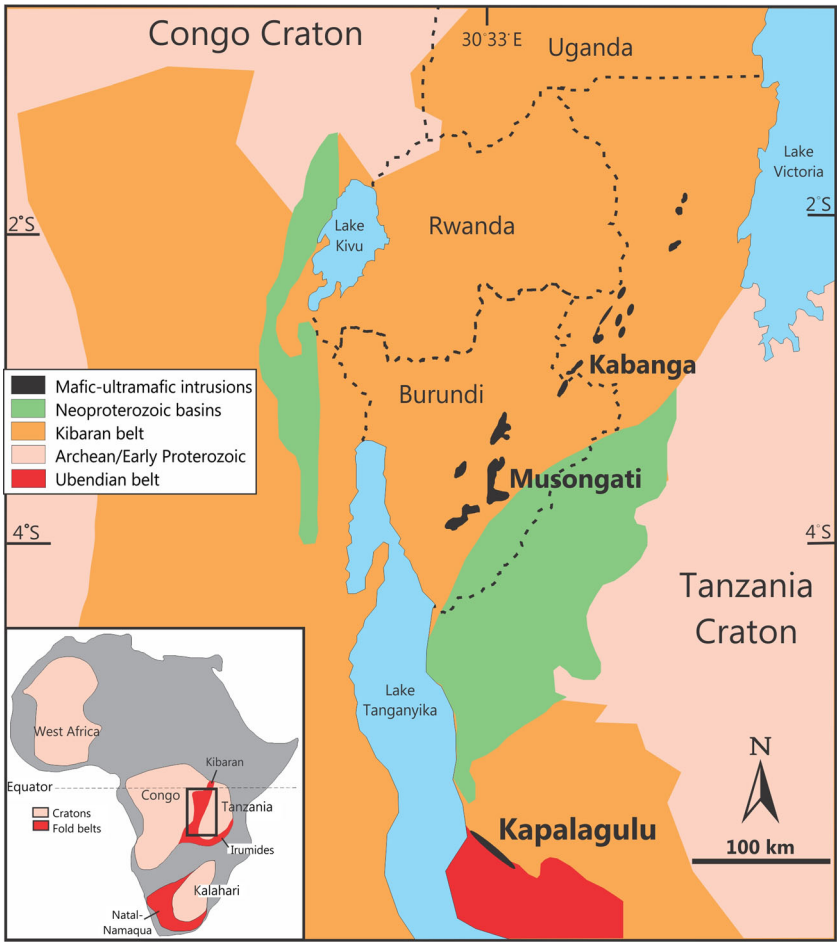

Fig. 1 Location of the Kapalagulu Intrusion with respect to other intrusions of the Central African Nickel Belt (after Maier et al. 2008) reproduced with the permission of the Mineralogical Society of Great Britain and Ireland from Cabri et al. (2015)

Kapalagulu Intrusion. They are best exposed on the sides of the prominent Kapalagulu Hill and it is here that Van Zyl (1956; 1959) identified a sequence of troctolite, lower gabbro, anorthosite, upper gabbronorite, magnetite gabbro, and banded gabbro with a stratigraphic thickness of about 1350 m that forms the Upper Mafic Sequence (Wadsworth et al. 1982; Wilhelmij and Joseph 2004; Maier et al. 2008).

Thrusting and high angle reverse faulting at the base of Kapalagulu Hill divides the Upper Mafic Sequence into the northern Makambo and southern Kapalagulu Structural Zones (Fig. 2). In these zones, the igneous stratigraphy dips eastwards and northeastwards below the overlying Itiaso Group metasediments. Underneath the Makambo Zone there is a poorly exposed sill of harzburgite and gabbro that most likely has a faulted contact with the gabbroic rocks of the Upper Mafic Sequence. Large rafts of Itiaso Group quartzite and graphite-bearing phyllite are present within the Makambo Sill and in the southeast form a screen between the sill and the Upper Mafic Sequence present in the Makambo Zone (Fig. 2). In places, the phyllite has undergone contact metamorphism implying associated thermal erosional melting and consequent sulfide contamination of magma (Maier et al. 2008).

To the southeast of the Upper Mafic Sequence exposed in the Kapalagulu Zone, there is an elongate dike-like body of ultramafic rock that forms the Lower Ultramafic Sequence of the Kapalagulu Intrusion, known as the Lubalisi Zone (Fig. 2). These ultramafic rocks are separated from the Kapalagulu Zone by a series of thrusts located at the base of Kapalagulu Hill, and with the exception of intermittent exposure along the

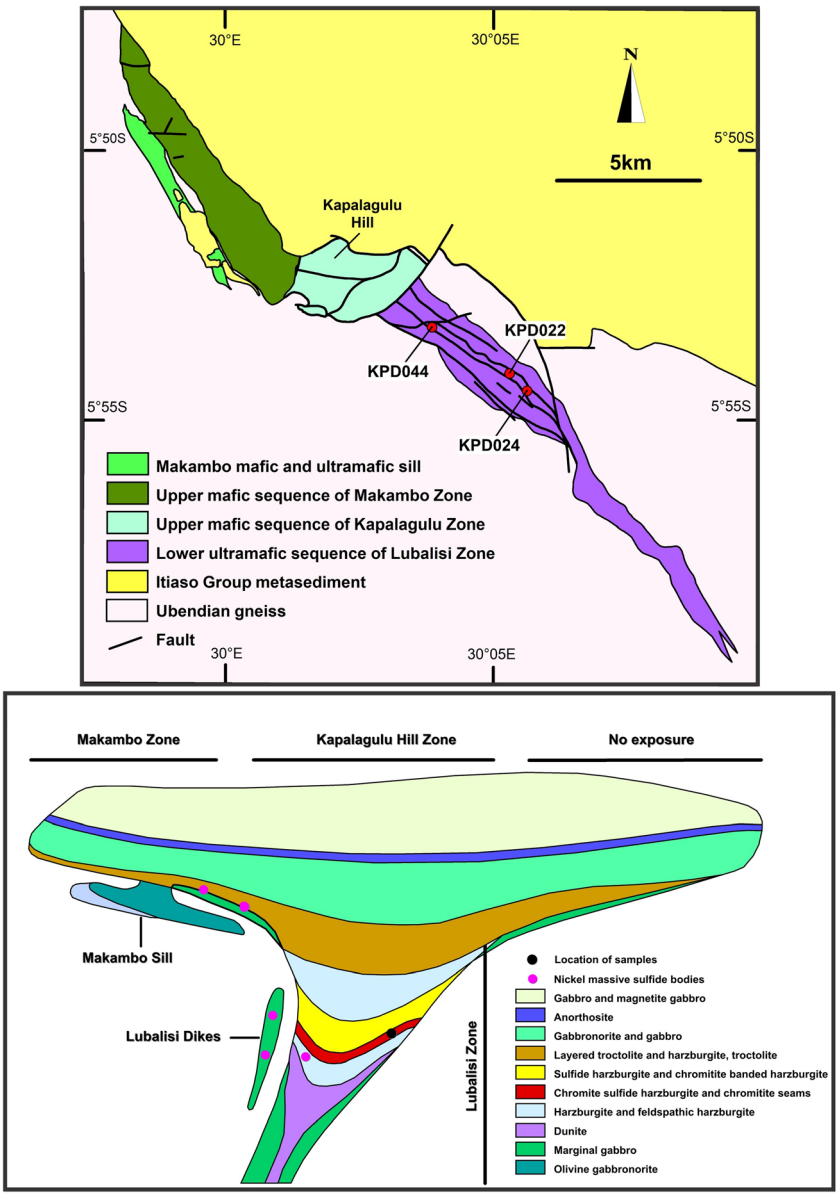

Fig. 2 *Bottom* A geological model of the Kapalagulu Intrusion showing the lower ultramafic and upper mafic igneous stratigraphy in relationship to the three structural and stratigraphic zones (Lubalisi, Makambo and Kapalagulu). *Top* the three structural zones of the Kapalagulu Intrusion showing the drill holes from which the samples were taken for PGM characterization

Lubalisi River and its tributaries, are blanketed by an undulating surface of laterite regolith. Deep diamond drilling by the Goldstream and Lonmin Joint Venture has identified an approximately 1550 m-thick sequence of dunite, harzburgite, and layered troctolite and harzburgite in the Lubalisi Zone. Thus, when including the Upper Mafic Sequence, the Kapalagulu Intrusion consists of a ca 3100-m-thick vertical sequence of layered ultramafic and mafic rocks. Except for a thin layer of basal harzburgite (10 to 100 m thick), the Lower Ultramafic Sequence is not well developed in the northern Makambo–Kapalagulu Zones (Fig. 2) and it is possible that faulting has removed the full extent of the lower sequence of ultramafic rocks in these structural zones.

The large-scale geometry of the Kapalagulu Intrusion appears to have the shape of a trumpet or wine glass, with the Makambo and Kapalagulu Zones representing the outward flaring of the intrusion over the dike-like Lubalisi Zone. A geological model showing this postulated intrusion geometry is shown in Fig. 2 and implies that folding and faulting associated with deformation of the Itiaso Group metasediments has resulted in the tilting of the trumpet-like structure towards the northwest. Also shown are the locations of the nickel massive sulfide bodies intersected by drilling that contain platinum mineralization and the approximate sample locations for the PGM study. In the geological model, the eastern extension of the Upper Mafic Sequence mirroring that was exposed in the Makambo Zone is thought to be buried beneath the eastward dipping succession of Makamba Formation phyllite and Mpeta Formation basal quartzite (Tack 1995; Deblond et al. 2001) that represents the roof of the intrusion. A gravity geophysical survey is needed to confirm this interpretation as a significant gravity anomaly would indicate dense gabbroic rocks buried below the less dense metasediments.

Structure of the Lubalisi Zone

As almost all of the ultramafic rocks that make up the Lubalisi Zone are obscured by a laterite regolith, it is only possible to reconstruct the internal structure and stratigraphy of the zone by identifying fault zones in drill core and the dips of lithological units (mostly chromitite bands and laminae) from the numerous deep-orientated diamond drill holes that were used to obtain intersections of the PGE mineralized harzburgite horizons (reefs). Geological information obtained from drilling shows that the Lubalisi Zone is 17 km long and more than 1000 m deep, and tapers to the south with the PGE mineralized harzburgite being confined to the widest portion (2 km) of the Lubalisi Zone immediately to the southeast of the Kapalagulu Zone. In this area, the layered ultramafic rocks form a syncline that plunges to the northwest towards Kapalagulu Hill (Fig. 3).

The geometry of the Lubalisi syncline has been modified by three major subparallel faults that dip steeply to the southwest and have been intruded by varying thicknesses of dolerite (Fig. 3). One of these faults, known as the Central Dolerite Fault is subparallel to the axial surface of the syncline. This is a rotational fault that in the southeast has a reverse sense (up-dip) movement and in the northwest has normal (down-dip) movement. There are two subparallel faults (Southern and

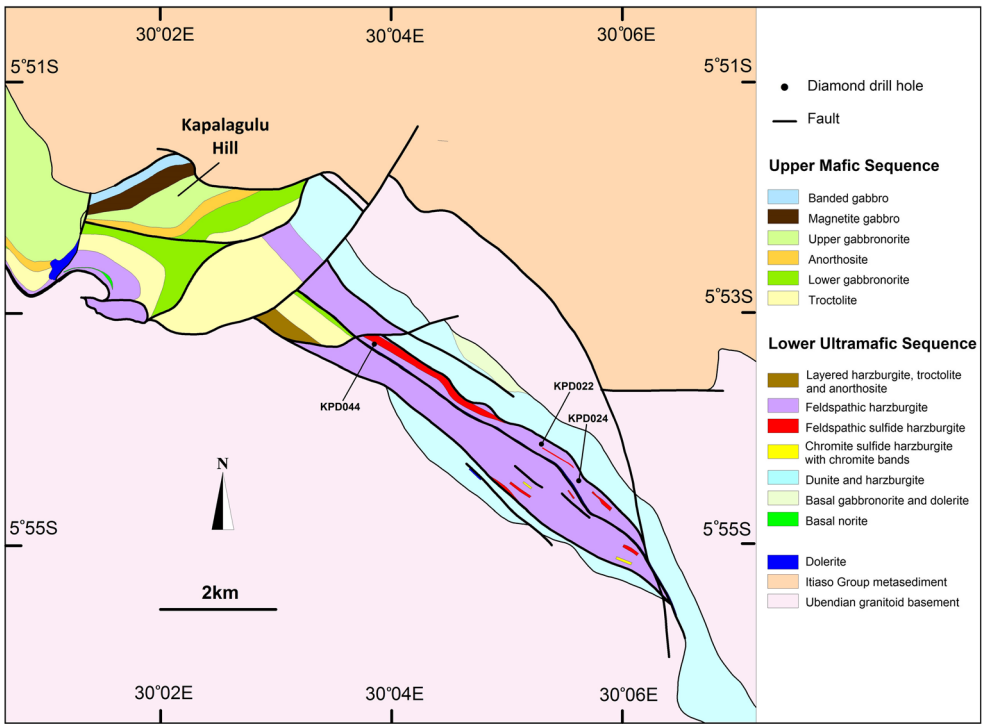

Fig. 3 Geology of the Lubalisi and Kapalagulu Zones outlining the Lower Ultramafic and Upper Mafic Sequences

Northern Faults) to the southeast and northwest of the Central Dolerite Fault which affect the ultramafic lithological layering in the southern and northern limbs of the Lubalisi Syncline. As the Southern Fault trends northwestwards towards Kapalagulu Hill, it progressively cuts downwards across the ultramafic igneous layering which finally results in a faulted contact between the Ubendian Basement and the Lubalisi Zone (Fig. 3).

Extensive drilling of the Main Chromite Sulfide Succession (MCSS), the harzburgite sequence which contains high-grade PGE mineralization, clearly outlines the synclinal shape of the lithostratigraphic unit which is confined to the northwestern part of the Lubalisi Zone where it has been further structurally modified by the axial Central Dolerite Fault. The MCSS is thicker in the southwestern limb of the Lubalisi Syncline in comparison to the northeastern limb, where the PGE grade is higher. This is illustrated in the three-dimensional diagram of Fig. A1 in Online Resource A which also shows the intrusion contact walls (partly faulted) with the Ubendian gneissic basement.

Drill holes have penetrated the gneissic wall and floor rocks along the southwestern contact of the Lubalisi Zone and show that there is an intrusive contact with extensive partial melting of the gneiss and the development of contaminated mafic and ultramafic rocks in the contact zone. Due to contact metamorphism, there is widespread retrograde metamorphism of the Ubendian gneiss (e.g., epidote alteration of garnet).

Stratigraphy of the Lubalisi Zone

The stratigraphy of the Lower Ultramafic Sequence preserved in the Lubalisi Zone of the Kapalagulu Intrusion was first described by Wilhelmij and Joseph (2004) who obtained lithological information from the exploration diamond drilling programs completed prior to 2004. Later drilling campaigns included a number of nearly 1000 m-deep vertical stratigraphic drill holes. The additional drill hole information resulted in a modification of the previously interpreted stratigraphy and a revised stratigraphic column (Fig. 4) using lithological information from five strategically located drill holes, up to 935 m deep, to the southwest of the Central Dolerite Fault. The approximately 1550 m vertical sequence shown in the stratigraphic column represents a northeast-dipping stratigraphic succession that forms the southwestern limb of the Lubalisi Syncline. Here, individual lithostratigraphic units are thicker than equivalents within the northeastern limb. The interpreted

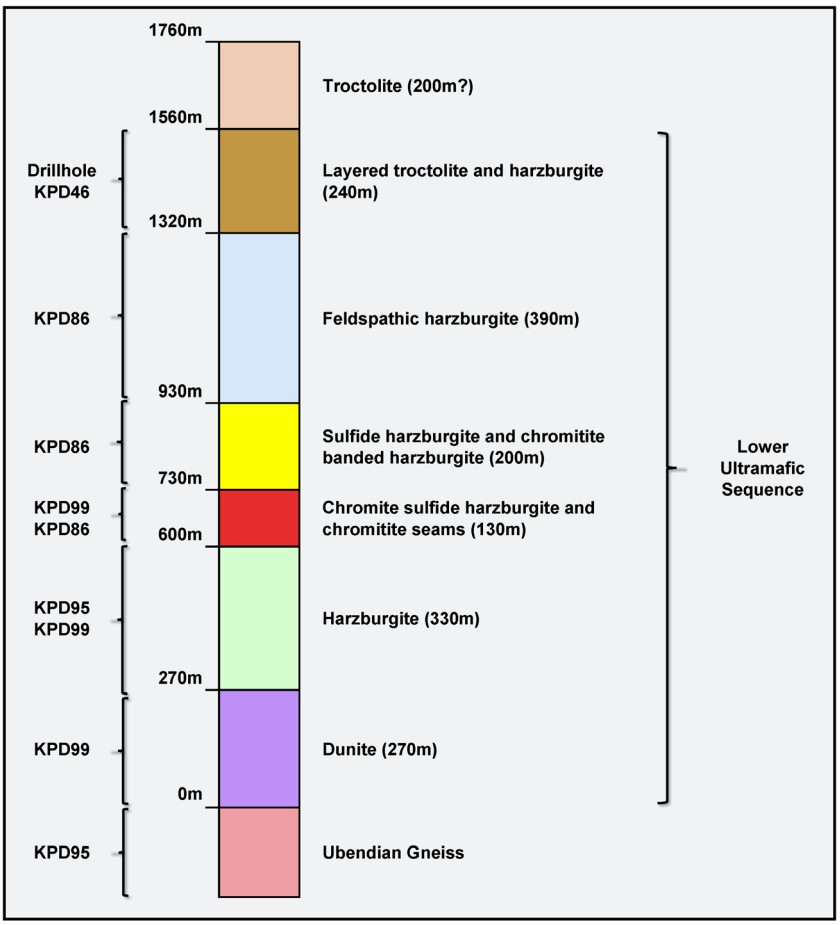

Fig. 4 Idealized stratigraphic column for the Lower Ultramafic Sequences of the Kapalagulu Intrusion in the Lubalisi Zone to the southwest of the Central Dolerite Fault

vertical stratigraphic sequence for the Lower Ultramafic Sequence is presented in Table D1 in Online Resource D and from the base upwards consists of six lithostratigraphic units known as the Basal Dunite, Lower Feldspathic Harzburgite, MCSS, Sulfide Harzburgite, Upper Feldspathic Harzburgite, and the Layered Troctolite and Harzburgite.

The fresh harzburgite samples for the PGM identification came from PGE reefs present in the MCSS located in the northeastern limb of the Lubalisi Syncline. This is where the highest grades of PGE mineralization occur associated with sulfide and chromite enrichment in reefs consisting of sulfide harzburgite (or dunite), sulfide-chromite harzburgite (or dunite) or individual chromitite seams and bands within the harzburgite. The MCSS lithostratigraphic unit is underlain by the Lower Feldspathic Harzburgite containing little sulfide and chromite mineralization and overlain by the Sulfide Harzburgite containing abundant disseminated and net-textured pyrrhotite, chalcopyrite, and pentlandite. In places there are intervals of chromitite bands within the Sulfide Harzburgite unit that contain low-grade PGE mineralization. In addition, there is widespread low to very low-grade PGE mineralization associated with the sulfides that characterize the Sulfide Harzburgite.

PGE mineralization in the MCSS harzburgite

Extensive diamond drilling of the harzburgite sequence within the Lubalisi Zone has identified stratiform PGE mineralization in thin reefs of chromite and sulfide enrichment near the base of the Lower Feldspathic Harzburgite that overlies the Basal Dunite, in the thin reefs of chromitite and chromite-sulfide harzburgite (or dunite) within the MCSS and as widespread low-grade mineralization associated with the Sulfide Harzburgite that overlies the MCSS. There is also high-grade PGE mineralization present within massive nickel sulfide bodies (some are differentiated) and thin veins present in the Lower Feldspathic Harzburgite located below the MCSS (Fig. 2) and within gabbro dikes present in the Ubendian basement close to the southwestern contact with the Lubalisi Zone. PGE mineralization is also present in thin remobilized sulfide veins associated with the Central Dolerite Fault. These other styles of PGE mineralization within the Lubalisi Zone that are not associated with the PGE reefs of the MCSS still need to be studied in detail. In the Lubalisi Zone, no PGE mineralization has been found in the Basal Dunite, Upper Feldspathic Harzburgite, and Layered Troctolite and Harzburgite.

Diamond drilling has concentrated on investigating the MCSS to determine the location and grade of the PGE mineralization that is associated with intervals of chromite and sulfide concentrations. This drilling has made it possible to outline the synclinal shape of the MCSS (Fig. A1 in Online Resource A), which is shown in the two cross-sections of Fig. 5. As illustrated in the cross-sections, the MCSS crops out beneath the laterite regolith along both limbs of the Lubalisi Syncline and is thickest within the southeastern limb and in the fold closure area (upper cross section of Fig. 5). Towards the northwest, fold axial parallel faulting within the southwestern limb of the syncline has resulted in the MCSS being buried beneath hangingwall harzburgite (bottom cross section of Fig. 5) which means that the surface expression of the MCSS is not as extensive to that present in the northeastern limb. Drilling shows that some of the very thick intervals of the MCSS are lenticular in shape and their three-dimensional geometry suggests that in places, the chromite-sulfide harzburgite fills channel-like structures (possible magmatic erosional structures) in the underlying feldspathic harzburgite that are up to 200 m deep.

Towards the end of the exploration campaigns, drilling of the MCSS focused on the northeastern limb of the Lubalisi Syncline where the lithological unit is thinner, has the greatest strike along the surface, and the grade of the PGE reefs is higher. Laterally impersistent PGE reefs represented by intervals of chromite- and sulfide-rich harzburgite and, or chromitite seams may contain high-grade PGE mineralization (e.g., 4.9 m at 1.88 g/t 3E including 0.15 m at 5.47 g/t from inclined drill hole KPD24). Consequently, due to the closely spaced drilling, more is known about the PGE distribution in the MCSS within the northeastern limb of the Lubalisi Syncline. In the southwestern limb of the Lubalisi Syncline, where the MCSS is thicker and the reef PGE mineralization is lower grade, there is development of copper and nickel mineralization associated with higher concentrations of disseminated and net-textured magmatic sulfides (chalcopyrite, pyrrhotite, and pentlandite).

Geological logging and sampling of drill core from the MCSS present in the northeastern limb of the Lubalisi Syncline shows that the PGE mineralization is intimately associated with the presence of chromite and/or sulfide in stratiform horizons of harzburgite, feldspathic harzburgite, and, in places, dunite where there is dominant cumulus olivine. Here, the PGE reefs within the MCSS occur at various stratigraphic levels, some near the base, others in the middle or at the top of the sequence. The PGE mineralized harzburgite or reefs are usually grouped together to form distinct vertical lithological units of varying thickness that may be either narrow (1 to 2 m) or wide (4 to 20 m). Individual chromitite bands and seams associated with the PGE reefs are laterally impersistent or form discrete packages in which there appears to be no recognizable pattern in the vertical arrangement of chromite- and sulfide-rich layers. In drill core, some of the chromitite seams are broken and disrupted, with rounded chromite enclaves (clasts) at some distance below the disrupted chromitite layer which implies lateral variability in both thickness and continuity.

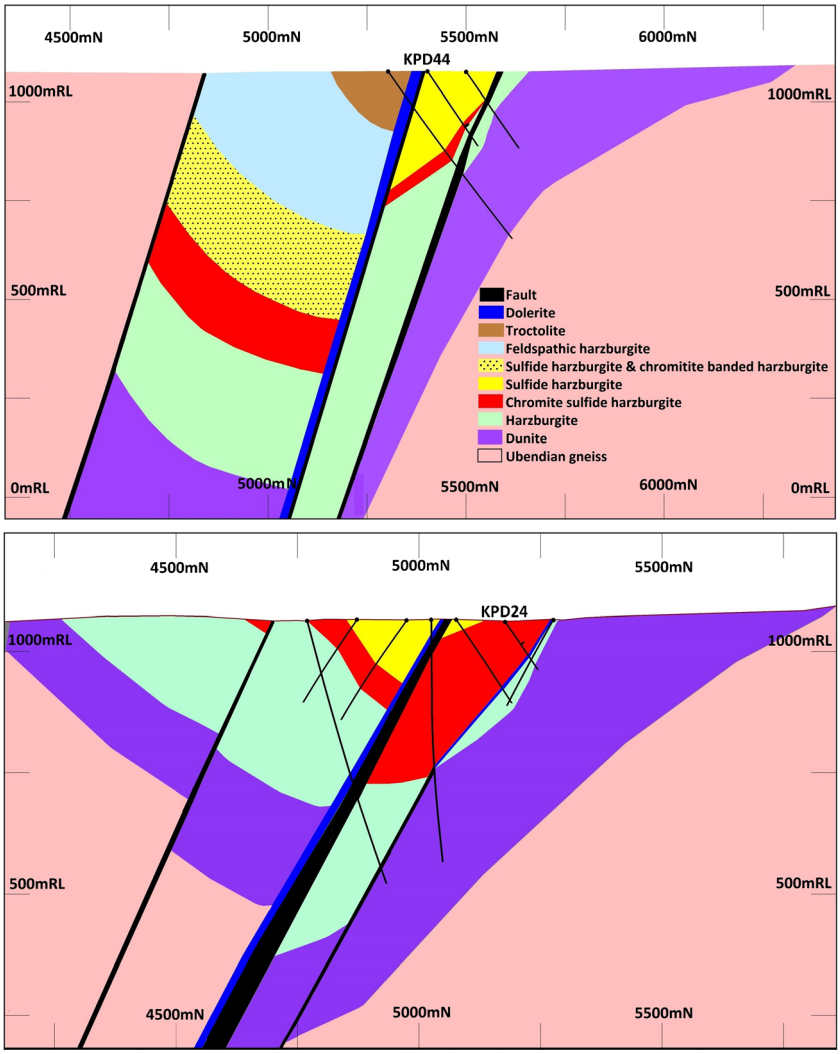

Fig. 5 Cross-sections of the Lubalisi Zone showing the location of the Main Chromite Sulfide Succession (*shown in red*) in the fold closure area of the Lubalisi Syncline (*bottom*) and in the northwest (*top*) showing the two drill holes (KPD44 and KPD24) from which samples were collected for PGM characterization

Using the presence or absence of visible chromite or sulfide, it is convenient to subdivide the PGE reefs within the northeastern MCSS into the following small-scale lithological associations, or end members:

1. Chromitite seams and bands
2. Chromite- and sulfide-bearing harzburgite
3. Sulfidic harzburgite with minor chromite

In the chromitite seams and bands and chromite-bearing harzburgite, there is invariably fine to very fine-grained sulfide that can be identified with a hand lens.

PGE reefs with chromitite seams and bands

In the chromitites of the northeastern MCSS, PGE mineralization can be confined to a single chromitite seam or to a series of chromitite bands over a narrow interval. However, the PGE mineralized chromitite is invariably associated with a much wider stratigraphic interval of PGE mineralization that includes chromite- and sulfide-enriched harzburgite above and below the chromitite seam.

Figure 6 shows an example of a 5-cm-thick (48.57 to 48.62 m) laminated chromitite seam from drill hole KPD23 that contains intervals of high-grade PGE mineralization (10.61 g/t, 10.15 g/t 3E). The narrow chromitite seam is underlain by PGE mineralized chromite harzburgite that together belong to a stratigraphic package (reef) of PGE mineralized harzburgite that is 4.10 m thick with an average grade of 1.77 g/t 3E.

The laminated chromitite is composed of six bands (5 mm wide) of fine-grained euhedral chromite with rounded partly serpentinized olivine and oikocrysts of plagioclase, orthopyroxene, and minor augite. Fine-grained disseminated sulfides occupy intergranular space and fractures in the chromite and olivine. In the chromite harzburgite underlying the laminated chromitite seams, the chromite consists of fine to medium-grained euhedral, or subhedral crystals that are disseminated within olivine, bronzite, and plagioclase. Fine-grained disseminated sulfide occupies intergranular positions

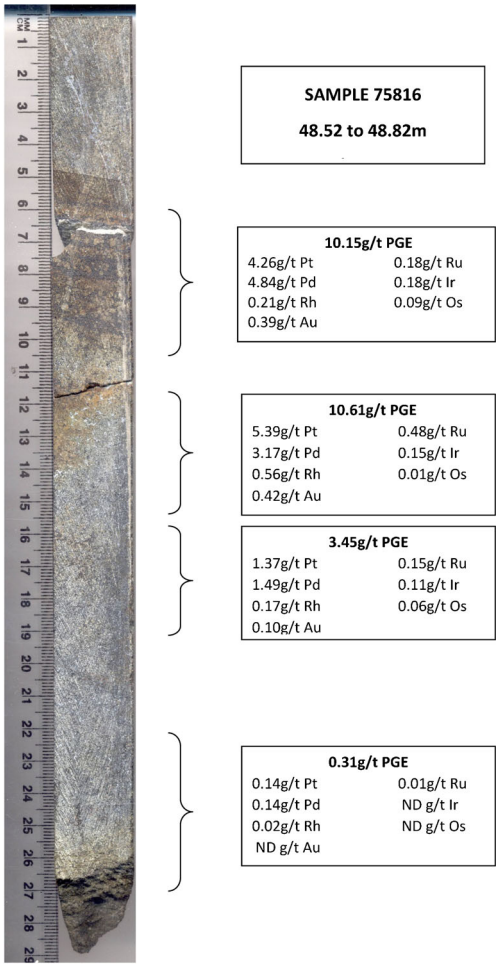

Fig. 6 Example of a laminated chromitite seam (*top of sample*) from drill hole KPD23 with high-grade PGE mineralization overlying chromite-sulfide harzburgite containing PGE mineralization that increase in value towards the basal contact of the seam

between closely packed olivine crystals and is often associated with, or included within, chromite crystals.

An example of a narrow interval of PGE mineralization associated with chromite-sulfide harzburgite containing chromitite bands is the intersection between 169 and 170 m for the KPD44 drill hole (Fig. A2 in Online Resource A). The PGE mineralized chromite harzburgite (90 cm at 6.25 g/t 3E) represents the highest PGE grade from a series of four thin horizons of chromite and sulfide enrichment over a 50 m-thick stratigraphic interval of harzburgite.

Two samples (D395 and D396) were taken from the high PGE grade intersections from KPD44 to characterize the PGM. Although the two samples have sustained some hydration, serpentinization and chloritization, the igneous textures are well preserved and the rocks are classified as chromite-bearing harzburgite. The cumulus minerals in the samples consist of olivine and chromite, the latter occupying interstitial volumes. The intercumulus assemblage is variable with the two most abundant intercumulus minerals represented by augite and plagioclase. Intercumulus clinopyroxenes are optically continuous, forming oikocrystic clinopyroxenes. Cumulus chromite is present as inclusions in both the intercumulus augite and plagioclase.

There is a marked modal variation, based on qualitative observations, in the amount of primary hydrous intercumulus minerals in this sample suite, with the hydrous minerals represented by phlogopite and lesser amounts of hornblende. Some phlogopite grains are oikocrystic.

In the secondary alteration, plagioclase is chloritized, olivine is serpentinized, and clinopyroxene is replaced by amphibole (tremolite)+magnetite, the latter a common alteration product of Fe-bearing clinopyroxene. Trace remobilization of sulfide is seen in serpentine-filled fractures.

Sulfide textures in the samples consist of sparsely distributed droplet-textured intercumulus sulfide (up to 2 mm in length) and sparsely disseminated minute monomineralic and polymineralic aggregates interstitial to cumulus chromite. The results of the PGM identification from the two samples are summarized and discussed in later sections.

PGE chromite and sulfide reefs

Within the MCSS, there are thick intervals of dunite (minor pyroxene) and sulfide harzburgite that contain PGE mineralization. For example, in the KPD24 drill hole there is an 8 m interval of PGE enrichment between 42.10 and 60.06 m (7.96 m at 1.87 g/t 3E) and it is possible to identify PGE distribution trends within this particular reef (Fig. A3 in Online Resource A). Here, there are five major peaks of PGE enrichment overlying an interval of lower-grade PGE mineralization and comments concerning the PGE mineralization follow.

1. There is a sympathetic increase of both palladium and platinum in the five peaks of PGE enrichment.
2. The lower PGE peak is associated with a pronounced interval of sulfide enrichment.
3. The upper four PGE peaks are associated with pronounced intervals of chromite concentration.
4. The uppermost PGE peak mineralization is associated with a chromitite seam (sample taken for PGM identification).
5. Beneath the interval of harzburgite containing the five PGE-rich intervals there is another interval of low-grade PGE mineralization that contains small peaks of PGE enrichment that are also associated with elevated amounts of sulfide and, to a lesser extent, chromite (not shown on diagram).
6. Overall, it is apparent that the PGE mineralization is closely associated with the presence of chromite and/or sulfide in the harzburgite.

Two samples were taken for PGM characterization from the PGE mineralized intersection from KPD24. They are from the laminated chromitite seam present between 52.7 and 53 m (sample 10369) and the feldspathic harzburgite located below the chromitite seam (sample 081914).

On closer petrographic examination, the chromitite seam (sample 10396) can be classified as a chromite-bearing dunite. The cumulus minerals include fine- to medium-grained equant-to-elongate closely packed olivine within interstitial cumulus chromite. The intercumulus mineral was plagioclase, which has been replaced by chlorite and sericite. There are local domains where the content of chromite is very low, however, the overall abundance of cumulus chromite distributed through the intercumulus volumes is uniform; aggregates of intercumulus chromite in interstitial volumes are interconnected. Locally, the chromite grains and aggregates appear to be concentrated in discontinuous layers. Minute quantities of intercumulus sulfide are present between cumulus chromite and trace amounts of sulfide have been remobilized in narrow hairline fractures.

The feldspathic harzburgite (sample 081914) can be classified as a sulfide-bearing chromite-rich dunite with the olivine and chromite being the principal cumulate minerals, after closer petrographic examination. There are trace amounts of cumulus sulfide within the closely packed medium-grained olivine which contains minor intercumulus plagioclase. Alteration of the olivine and plagioclase is minimal. Sulfide inclusions are present within both the olivine and chromite indicating early sulfide saturation of the parental magma. Chromite inclusions are also present in some of the olivine grains.

There are approximately equal proportions of pyrrhotite and pentlandite amongst the sulfide grains which include minor chalcopyrite and rare sphalerite. These sulfides occur mostly as disseminated monomineralic grains and polymineralic aggregates interstitial to chromite and as droplet-textured polymineralic aggregates. The results of the PGM characterization for the two samples are summarized and discussed in later sections.

Comparison of MCSS harzburgite reefs

In the MCSS lithostratigraphic unit of the Lower Ultramafic Sequence preserved in the Lubalisi Zone of the Kapalagulu Intrusion, there are stacked intervals (reefs) of PGE mineralization associated with chromite-sulfide horizons that display a wide variety of magmatic structures that include chromitite seams, multiple chromitite bands, disrupted chromitite bands and seams, rounded chromitite enclaves and other enigmatic structures that are only partially revealed in the drill core. The PGE mineralized harzburgite of the MCSS forms part of a very thick stratigraphic sequence of harzburgite that is underlain by dunite and overlain by layered troctolite and harzburgite. Together these stratified ultramafic rocks of the Lower Ultramafic Sequence in the Lubalisi Zone represent the infilling of a narrow dike-like subchamber that underlies a more extensive upper magma chamber filled by the well- layered gabbroic rocks of the Upper Mafic Sequence preserved in the Kapalagulu and Makambo Zones of the Kapalagulu Intrusion.

In conclusion, the PGE reefs of the Lubalisi Zone are in the middle of an approximately 1500 m-thick sequence of stratified olivine-rich ultramafic cumulate rocks and have some geological and geochemical features that are similar to the PGE-bearing Main Sulfide Zone (MSZ) of the Great Dyke, the Main Sulfide Sequence (MSS) of the Munni Munni Complex, the Lower and Upper Group chromitites (that include the UG2 Reef) and Merensky Reef of the Bushveld Complex, as well as other layered intrusions which contain PGE-bearing reefs (Maier 2005). Comparisons between the MCSS reefs and these other well-documented PGE reefs are discussed in further detail in the concluding section.

PGE mineralization in Lubalisi Zone laterite

Extensive shallow air core drilling (160 drill holes) of the laterite regolith that covers most of the Lubalisi Zone has outlined substantial nickel and PGE mineralization. Results from the widespread drilling of the laterite shows that the high-grade areas of PGE (>1 g/t 3E) and Ni (>0.8 %) are associated with the harzburgite protolith lithostratigraphic units that contain concentrations of sulfide and chromite. These are the MCSS which contains the PGE reefs and the overlying Sulfide Harzburgite lithostratigraphic unit. The spatial distribution of the higher grade Ni and PGE laterite is shown in Fig. 7. It clearly outlines the synclinal surface trace of the sulfide and PGE mineralized harzburgite protolith associated with the Lubalisi Syncline.

The Lubalisi Zone of the Kapalagulu Intrusion is located on an undulating plateau that has been incised by the Lubalisi River and its tributaries. The plateau is bounded in the northeast by an escarpment formed by the erosionally resistant Itiaso Group metasediments (Tack 1995) and in the southwest by another escarpment that steps down to Lake Tanganyika that is related to extensional graben-forming faulting. There has been a prolonged period of tropical lateritic weathering of the rocks that make up the Lubalisi plateau with the development of a thick laterite profile over the ultramafic rocks of the Lubalisi Zone which are more susceptible to chemical weathering in comparison to the quartz-rich Ubendian gneiss. In the Lubalisi Zone, the development of an erosionally resistant ferricrete horizon at the top of the laterite profile has preserved the soft underlying saprolitic clays from fluvial erosion. It is possible to determine the internal stratigraphy of the laterite by digging pits and trenches within the sides of eroded

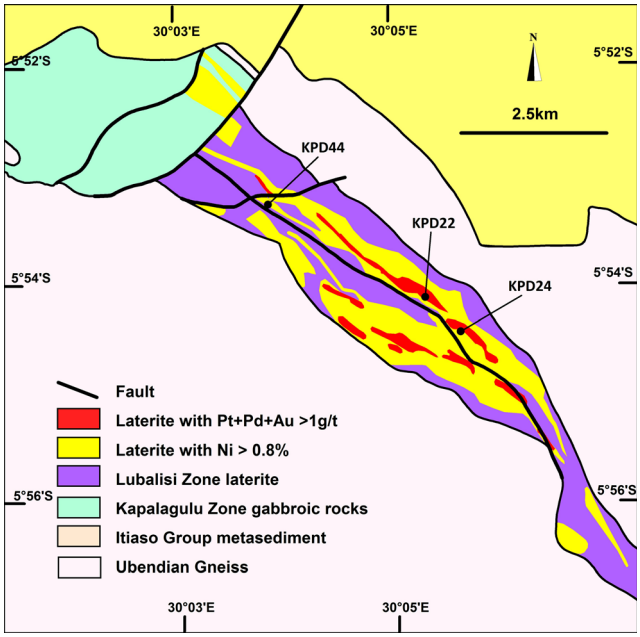

Fig. 7 Location of the 0.8 % Ni and 0.5 g/t 3E cut-off laterite Ni and PGE resources in the Lubalisi Zone

fluvial tributaries of the Lubalisi River where the hard ferricrete cap has been removed by stream erosion. It was in one of these trenches that BHP discovered PGE-bearing chromitite bands of weathered harzburgite saprock below the ferricrete. However, the drilling of numerous shallow air core holes has made it possible to identify the lithological units that make up the Lubalisi Zone regolith over a wide area by the geological logging of recovered drill chips.

The laterite regolith of the Lubalisi Zone is composed mostly of oxides of iron and aluminum. From the weathered saprock upwards, the laterite consists of four stratigraphic horizons, these being saprolite clay, ferruginous red clay (ferralite), pisolitic ferricrete (duricrust), and red laterite soil (Fig. A4 in Online Resource A). These horizons can interfinger with each other and the thickness varies according to topography. Geochemically, they represent an accumulation of Fe_2O_3 and Al_2O_3 and a partial to total loss of SiO_2 and MgO. It is important to note that the horizons differ from each other in color, grain size, density, and chemical content.

Drilling in the Lubalisi Zone shows that the weathered and oxidized saprock can consist of either basement granite—gneiss, dunite, serpentinite, harzburgite, or gabbronorite. In places, where the overlying lateritic regolith has been removed by recent fluvial erosion, the saprock is covered directly by lateritic soil.

The saprolite is located at the base of the lateritic profile and the pH of the zone is alkaline due to liberation of the Ca and Mg from the host dunite and harzburgite. By definition, the saprolite has a recognizable primary structure and is medium to coarse-grained at the base and fine-grained and friable at the top. Depending on the protolith, the saprolite is either yellow, yellow-orange or yellow-green in color. It is possible to recognize granitoid saprolite, ferruginous saprolite after harzburgite, yellow-green saprolite after dunite-serpentinized dunite and yellow-orange saprolite after feldspathic harzburgite.

At the base of the saprolite horizon, there are partly decomposed fragments of dunite or harzburgite and geological logging of diamond drill core shows that in places there are veins, fractures, and voids filled by nickel-bearing "garnierite" (generic name used for green mineralization in laterites) and black veinlets of manganese wad from colloidal precipitation. The saprolite is characterized by clay minerals of the montmorillonite group and serpentinite. As the saprolite is porous, it has a low density (about 1 g/cm^3).

In the red-brown structureless ferruginous clay horizon that overlies the saprolite, there is concentration of iron and aluminum and loss of silica and magnesium. The clay is friable and plastic and grades upwards into the ferricrete horizon by the development of pisolites and colloform-textured goethite and hematite. In contrast to the saprolite, there tends to be a collapse of pore spaces in the ferruginous clays and a reduction in volume. The ferruginous clay thus has a higher density to that of the saprolite.

The ferricrete horizon which overlies the ferruginous clay is characterized by its greater hardness and higher density (1.4 to 2 g/cm^3). It is composed of pisolitic limonite and goethite which gives the lithology a botryoidal appearance. The ferricrete was formed by the precipitation of soluble iron present in rising and falling groundwater to form insoluble iron hydroxides.

The lateritic soil is red-brown in color and can be either residual or resedimented when containing sand and pebbles. When residual, the lateritic soil consists of either reconsolidated fine-grained lateritic pisolites and indurated lateritic soil or red clay. The transition from the soil into the underlying ferricrete is gradual and is defined by an increase in the presence of cemented ferruginous pisolites. In places, the interface between the soil and ferricrete is defined by a change in color from red to yellow-brown.

Drilling of closely spaced vertical holes through the Lubalisi laterite showed that it is possible to trace the PGE reefs in the MCSS up-dip into the laterite profile where there has been a concentration of chromite and PGE in the saprolite clay. A cross section for the KPD22 drill hole from which samples were taken for PGM characterization in the regolith is shown in Fig. 8. This illustrates the spatial concentration of Ni and PGE in the regolith. The Ni is concentrated in the saprolite above the harzburgite saprock and protolith. In contrast, the PGE are concentrated in the ferruginous red clay and upper saprolite clay which represents the up-dip remnants of PGE reefs containing chromite and sulfide harzburgite associated with the MCSS lithostratigraphic unit. Large amounts

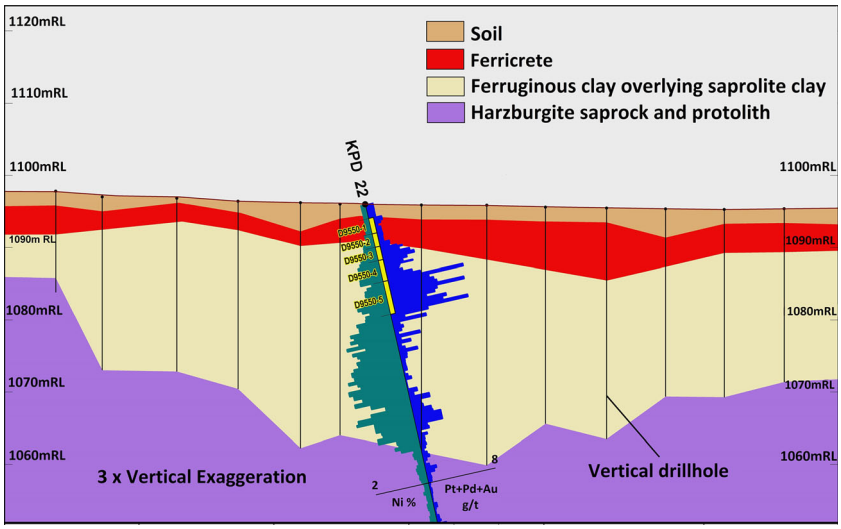

Fig. 8 Location of samples with respect to the lateritic regolith units intersected in the KPD022 drill hole. The vertical lines are air core drill holes and there is three times vertical exaggeration

of residual chromite are associated with the PGE laterite mineralization reflecting the close relationship between PGE and chromite in the harzburgite protolith. It is likely that the PGE in the laterite regolith represent residual concentration that included some supergene processes such as remobilization of the more susceptible PGE due to surface chemical weathering. This is discussed further in the concluding section.

Sample locations and methodology

Sample locations

Four unoxidized sulfide-bearing samples were studied, comprising two contiguous samples from DDH KPD44 (D-935 and D-396, each 30 cm long) and two others, 2.86 m apart, from DDH KPD24 (081914 [15 cm long] and 010369 [30 cm long]). See also Online Resource A (Figs. A2 and A3). Five oxidized samples from drill core KPD22 were taken from 2.4 to 18.5 m depth. An idealized 20.2-m-thick PGE-bearing laterite regolith is shown in Online Resource A (Fig. A4) and precious metals, base metal and chromium distribution for the lateritic sample intervals taken from KPD22 are shown in Online Resource A (Fig. A5).

Sample preparation

The initial sample preparation of the sulfide-bearing samples was different to the oxidized samples. A slice for petrography and ore microscopy was cut from each of four sulfide-bearing samples; the remainder was crushed and quartered. Splits from the four samples were taken for modal analyses of major/minor minerals, grain-size analysis, and liberation characteristics of the minerals by automated image analysis (Cabri and Wilhelmij 2015), but there was sufficient material for only three samples (D-395, D-396, and 10369) for gravity concentration by hydroseparation[1] (see, for example, Cabri et al. 2005). The weights of the splits and after screening at 45, 75, 125, and 180 μm are given in Online Resource F, Table F1. Some automated searches for platinum-group minerals (PGM), done after completion of the hydroseparation/SEM study used the methodology described in Lastra et al. (1999).

Oxidized samples were subjected to a more complex preparation process to separate some of the clay minerals as shown in a flow chart (Online Resource B, Fig. B1); the weights of splits after attrition milling are given in Online Resource F, Table F2. Attrition is a surface phenomenon where shear stress causes material to abrade off and is sometimes used to activate mineral surfaces for subsequent flotation (e.g., Rabatho et al. 2011).

Concentration, search for, and analyses of minerals

The sized and screened subfractions of the sulfide-bearing samples, prior to concentration by hydroseparation, were treated separately until the purest concentrate was achieved. The aliquots of "grit" (after attrition) of oxidized samples were further processed by "grinding" with a finger (under water) and decanting the clay-size fractions, which were quite abundant because the initial hydroseparation indicated that the material still contained a lot of fine-grained clay-size particles. The reground tailings were then wet-sieved at 40, 63, 80, and 200 μm and further polished sections were made of hydroseparation concentrates.

The hydroseparation concentrates were first tested by mounting 0.1 g (or less) as a monolayer in a 2.5 cm polished section and checking for the number of PGM particles using a Camscan Microspec-4DV scanning electron microscope with

[1] Using an earlier manual model of hydroseparator (HS-01).

a Link AN-1000 detector. All the concentrates for the different fractions were then completely scanned and precious-metal minerals and major sulfides found were identified by electron probe microanalysis (EPMA) and imaged for later off-line area measurements. The area of each precious-metal mineral was measured manually using the "ImageJ" program (except for some scanned by quantitative image analysis). The area of the precious-metal mineral (measured in square micrometers) and the equivalent circle diameter (ECD) was calculated for each grain. The volumes and masses of Pt, Pd, and Au were then calculated, as represented by each grain, using ideal calculated densities for PGM. The densities used for the Au-Ag alloys are based on the data of Kraut and Stern (2000). The abundances of PGM are reported as weight % of the total PGM and not of each sample, thus they represent in reality relative weight % or relative abundances.

Selected grains of pentlandite and pyrrhotite/troilite from the sulfide samples were also analyzed using the Camscan-4DV SEM with Microspec-3PC wavelength-dispersive spectrometer. Trace analyses for Pd were also done on pentlandite grains using a 20 kV accelerating voltage, 250 nA beam current with 60 s counting time for a calculated detection limit for Pd of 50 ppm. A JEOL 8900L electron microprobe was used for analyses of oxide and silicate minerals with all analytical details given in Online Resource F, Table F5.

X-ray diffraction analysis

Qualitative X-ray diffraction (XRD) was done on the sulfide samples prior to image analysis in order to allocate compositions for the major minerals. For the clay samples, water suspensions were pipetted onto glass slides and air-dried overnight to produce oriented mounts. X-ray patterns of the air-dried samples were recorded on a Bruker D8 Advance Powder Diffractometer equipped with a graphite monochromator, Co Kα radiation set at 40 kV and 40 mA. The samples were also X-rayed following saturation with ethylene glycol and heat treatment (550 °C). The samples were extremely Fe-rich and hence did not produce patterns suitable for detailed analyses. Also, there were no reference minerals available for the minerals contained here. Thus, only qualitative analyses were carried out. In addition, the samples needed to be reground to yield a better pattern. Two samples were reground for over an hour in a small ball mill and re-analyzed.

Platinum-group minerals from the MCSS harzburgite

Assays and mineralogy

Assays and field lithology of the four samples are given in Table 1. The samples are chromite-rich, with over 25 wt% chromite, except for sample D396, which contains ~10 wt% chromite. The principal silicate minerals are lizardite, clinochlore, forsterite, and enstatite. Samples D395 and D396 contain more of the first two minerals, which confirms their classification as peridotite/wehrlite and samples 81914 and 103069 contain more of the latter two minerals, confirming their classification as chromite-rich dunite.

The most common sulfide and oxide species in the HS concentrates, often found associated with PGM, are listed in Online Resource F (Table F3). Monoclinic pyrrhotite and troilite were found to contain no Ni and

Table 1 Chromite-sulfide harzburgite samples

Hole and Sample ID	From (m)	To (m)	Pt+Pd+Au ppm	Pt ppm	Pd ppm	Pt/Pd	Au ppm	Cr %	Cu %	Ni %	S %	Lithology
KPD24 10369	53.00	53.30	5.57	1.82	3.63	0.50	0.13	6.47	0.08	0.32	0.30	Chromitite seam with 20–40 % chromite and 1 % sulfide. Harzburgite base
KPD24 81914	56.16	56.31	4.49	1.99	2.03	0.98	0.48	6.01	0.10	0.36	0.50	Chromite harzburgite with 10–20 % chromite and 2–3 % sulfide
KPD44 D395	169.30	169.60	11.57	3.48	7.97	0.44	0.12	6.08	0.21	0.46	0.80	Chromite-sulfide harzburgite with bands of fine-grained chromitite
KPD44 D396	169.60	169.90	4.20	0.94	3.03	0.31	0.23	2.38	0.22	0.44	0.90	Chromite-sulfide harzburgite with bands of disseminated chromitite

KPD24 (Dip: −55°; Azim: 27.5°; 30° 05′ 37″ E, 5° 54′ 26″ S) and KPD44 (Dip: −56°; Azim: 29°; 30° 03′ 51″ E, 5° 53′ 16″ S)

pentlandite was found to contain trace concentrations of Pd. Using the pentlandite quantities determined by image analysis of the crushed samples, the deportment of Pd in pentlandite was calculated to represent 13.5, 18.0, and 21.0 % of the total Pd for samples D395, D396, and 10369, respectively.

A total of 134 PGM particles were measured in sample D395, most of which were found in the −45 μm fraction, consisting of 15 PGM species, in addition to "electrum" (Au,Ag) and a single hessite ($AgTe_2$) particle. The most abundant PGM is sperrylite ($PtAs_2$) followed by sobolevskite (ideally PdBi), moncheite (ideally $PtTe_2$), and michenerite (ideally PdBiTe). Less common are tetraferroplatinum (ideally PtFe), atokite (ideally Pd_3Sn), isoferroplatinum (ideally Pt_3Fe), "mertieite" (a Pd-Sb-As mineral), kotulskite (ideally PdTe), cooperite (ideally PtS), vysotskite (ideally PdS), a PdCu alloy, now considered to be skaergaardite, plumbopalladinite (ideally Pd_3Pb_2), sopcheite (ideally $Ag_4Pd_3Te_4$), and an unknown alloy with a composition of Pd_3Ni.

A total of 93 PGM and Au minerals were found in sample D396 (mostly in the −45 μm fraction), consisting of about 14 PGM species, in addition to "electrum" and aurostibite ($AuSb_2$). The most abundant PGM is sperrylite ($PtAs_2$) followed by the PGE bismuth-tellurides [maslovite (ideally PtBiTe), michenerite (ideally PdBiTe), keithconnite (ideally $Pd_{20}Te_7$), moncheite, kotulskite], sobolevskite, atokite, native palladium, an unknown Pd alloy (Pd_3Ni), a second occurrence of a new PGM (Pd_2Si),[2] laurite (ideally RuS_2), a Pt-Ru-Rh sulfide, a Pd-Ag-telluride (possibly a new mineral), and menshikovite (ideally $Pd_3Ni_2As_3$). Analysis of the Pd-Ag telluride gave $Pd_{0.99}(Ag_{0.85}Pb_{0.19}Ni_{0.02}Cu_{0.01})_{\sum 1.07}(Te_{0.91}Se_{0.03})$, which may represent another new mineral with an ideal formula of PdAgTe though this composition was not reported in a recent study of the Ag-Pd-Te system by Vymazalová et al. (2015).

A total of 137 PGM, Au, and Ag minerals were found in the various HS concentrates of sample 10369, including some particles found separately by image analysis. In addition to "electrum", a Ag>Au alloy and a single occurrence of native silver were also recorded. The PGM consist of about 15 species, in addition to the Au and Ag alloys. Sperrylite is most abundant in terms of mass, followed by PGE and Au alloys, and then by the PGE bismuth-tellurides and tellurides (moncheite, kotulskite), sobolevskite, keithconnite, the Pd-Sb-As minerals, including the Pd-Sb minerals ["mertieite", stibiopalladinite, sudburyite (ideally PdSb), genkinite (ideally $(Pt,Pd)_4Sb_3$)] atokite, native palladium, isoferroplatinum, the unnamed Pd_2Si (palladosilicide), and maybe vysotskite (ideally PdS). One small 2.7-μm particle of stibiopalladinite is Ag-bearing with a possible composition of $Pd_{4.89}(Sb_{1.63}Ag_{0.48})$. All measurements for the all precious-metal minerals found in this sample are listed in Cabri et al. (2015, Table 1). Figure 9 shows that just three PGM and Au minerals, from 32 to 64 μm in size, account for 32 wt% of the PGM and Au minerals; selected backscattered scanning electron microscope (SEM) are given in Fig. 10.

The precious-metal minerals found in the heavy mineral hydroseparation concentrates for samples D395 and D396 are listed in Online Resource E, Tables E1 and E2, together with the frequency, relative mass% and volume% for each mineral, and the particle sizes for each sample (P80 and P50). Selected SEM photomicrographs of the precious-metal minerals for two of the samples are given in Online Resource C (Figs. C1 and C2). The trace analyses of Pd in pentlandite are listed in Online Resource F, Table F4.

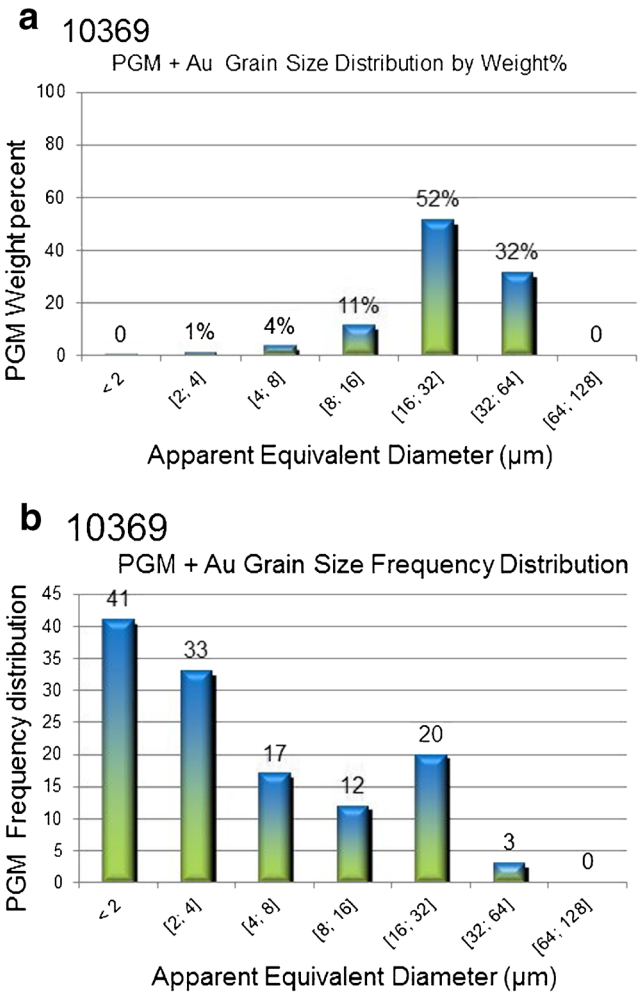

Fig. 9 PGM and Au minerals grain-size distribution by weight % (a) and frequency (**b**), (10369, n=137)

[2] The mineral was recently characterized and approved by the IMA as palladosilicide (see Cabri et al. 2015).

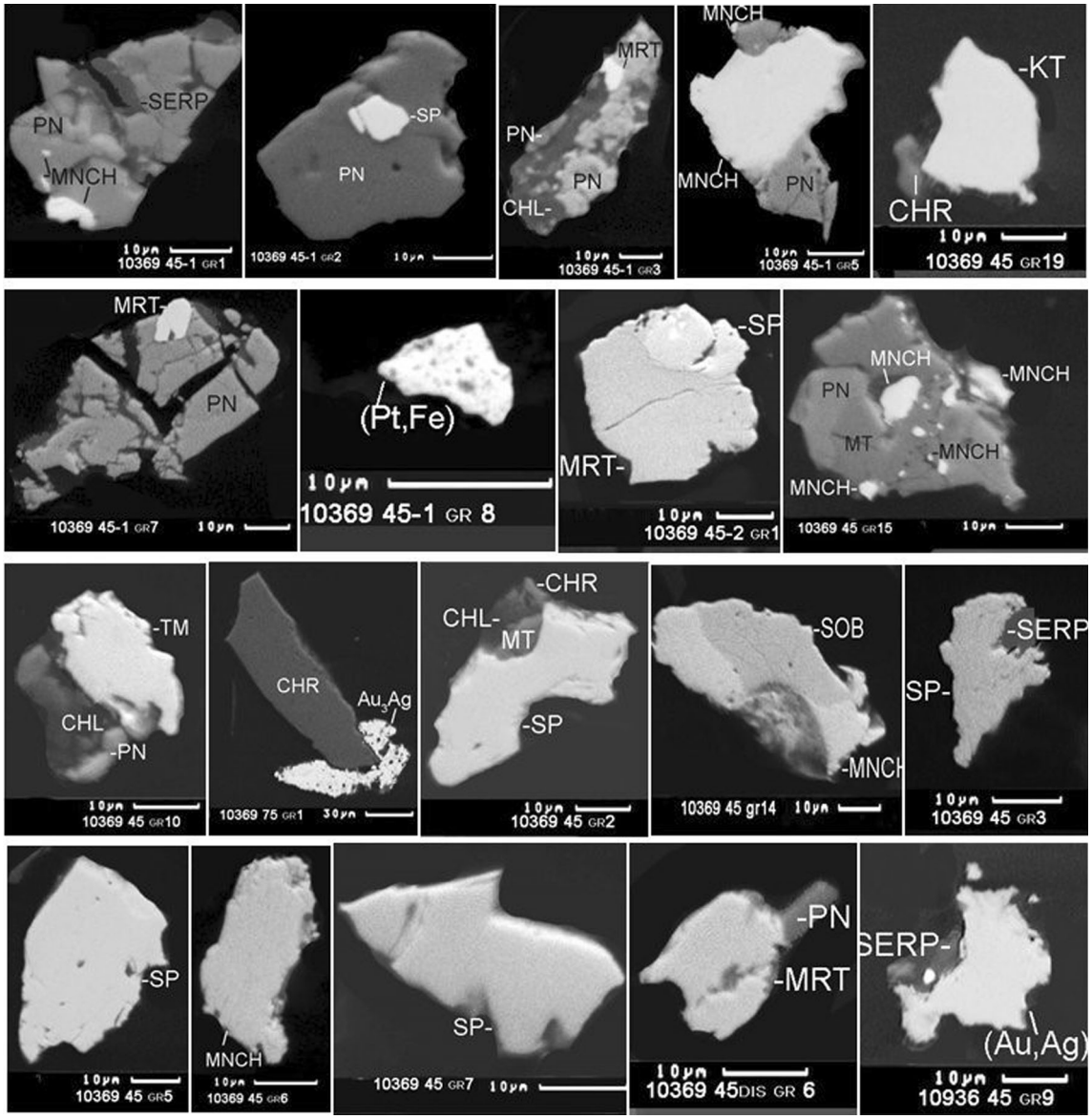

Fig. 10 SEM photomicrographs of selected precious-metal minerals, sample 10369. Abbreviations: *Au,Ag* electrum, *CHL* chlorite, *CRT* chromite, *KT* kotulskite, *MNCH* moncheite, *MRT* mertieite II, *MT* magnetite, *PN* pentlandite, *SERP* serpentine, *SOB* sobolevskite, *SP* sperrylite

Platinum-group minerals from the Lubalisi Zone laterite

Assays and mineralogy

Assay data keyed to lithology was provided by Goldstream Mining NL (Table 2). After attrition milling, 100 g sample splits of "grit" and "clay" were assayed by Genalysis Laboratory Services Pty Ltd (Online Resource D, Table D2). The five samples consist mainly of the same phases, but in variable concentrations, as seen in an exploratory SEM investigation. The matrix consists of a very fine-grained mixture of iron oxides (goethite and hematite), clay-size minerals (i.e., <2 μm in size), and clay minerals (and possibly quartz). This mixture cements and encloses larger particles and grains of the other minerals. Quartz is often rimmed by goethite; in deeper samples it is often corroded in appearance, with various oxides filling the corrosion cracks. The distinction between goethite [ideally α-FeO(OH)] and hematite (ideally Fe_2O_3) was made on the basis of texture and composition. Hematite is usually pure iron oxide with little Al or Si and has a uniform appearance in backscattered mode (average analyses are given in Table 3). Goethite usually has significant Al and/or Si and is texturally complex (average analyses are given in Table 3), with obvious banding or botryoidal features (e.g., Online Resource C, Fig. C3a). Hematite often has round bubble-like voids. The proportion of hematite drops substantially in the samples with increased depth.

Table 2 Laterite regolith samples KPD22 (assays weighted by length)

Hole and Sample ID	From (m)	To (m)	Pt+Pd+Au ppm	Pt ppm	Pd ppm	Pt/Pd	Au ppm	Cr %	Cu %	Ni %	Fe%	Lithology
D9550-1	2.4	5.0	1.1	0.6	0.4	1.5:1	0.1	1.7	0.1	0.2	36.7	Ferricrete
D9550-2	5.0	7.3	1.2	0.5	0.5	1.0:1	0.1	3.1	0.1	0.4	34.0	Red clay
D9550-3	7.3	9.5	2.8	1.3	1.3	1.0:1	0.3	4.6	0.2	0.6	35.5	Chromite saprolite clay
D9550-4	9.5	13.0	2.8	1.2	1.4	0.8:1	0.2	4.5	0.3	0.8	34.9	Chromite saprolite clay
D9550-5	13.0	18.5	5.9	2.7	2.7	1.0:1	0.5	6.9	0.3	0.9	37.7	Chromite saprolite clay

KPD22 (Dip: −55°, Azim: 29°; 30° 05′ 18″ E, 5° 54′ 7.6″ S)

Goethite is a major component in all samples, although its habit changes from surface with depth. In sample 9550-1, goethite mainly occurs as banded masses of intimately mixed goethite and halloysite ($Al_2Si_2O_5(OH)_4$), e.g., Online Resource C, Fig. C3a. With increased depth, a latticework type of goethite presumably formed from the breakdown of hematite/sulfide grains becomes predominant (e.g. Online Resource C, Fig. C3b). Halloysite is fairly common in all samples, but its mode of occurrence changes. In the samples nearer the surface, it mainly occurs as very fine grains in the matrix and intimately mixed with hematite/goethite (Online Resource C, Fig. C3c, 9550-1). As sample depth increases, halloysite is increasingly found as larger, separate grains with complex compositional features observable in backscattered electron images (Online Resource C, Fig. C3d, 9550-3). Chromite occurs in all samples as rounded to subhedral grains. The size and modal concentration of chromite increase substantially with increasing sample depth. In sample 9550-1, chromite is an accessory phase (4 %),

Table 3 Microbeam analyses of chromite, hematite, and goethite (wt. %)

Sample#	*n*	MgO	NiO	MnO	TiO_2	SiO_2	Al_2O_3	ZnO	FeO	CaO	V_2O_3	Cr_2O_3	Total
Average chromite													
9550-1	14[a]	6.70	0.13	0.38	2.28	0.02	12.37	0.16	34.29	–	0.41	42.56	99.30
9550-2	10	7.10	0.15	0.37	2.47	0.02	13.60	0.11	34.28	–	0.41	40.51	99.04
9550-3	12[b]	7.71	0.11	0.35	1.55	0.05	13.95	0.13	30.44	–	0.31	44.88	99.48
9550-4	10[c]	8.21	0.13	0.32	2.03	0.03	15.81	0.10	30.12	–	0.32	42.88	99.96
9550-5	16[d]	7.60	0.13	0.30	1.59	0.05	14.76	0.10	30.20	–	0.30	44.06	99.08
Std. dev.		0.581	0.014	0.034	0.409	0.015	1.287	0.025	2.211	–	0.055	1.663	0.374
Average hematite													
9550-2	5	0.09	0.22	0.27	0.33	1.24	5.27	0.01	75.14	0.07	0.06	4.44	87.14
9550-3	5	0.06	0.43	0.22	0.35	1.21	5.42	0.03	71.01	0.04	0.12	7.67	86.56
9550-4	5	0.04	0.27	0.20	0.50	1.53	5.21	0.01	72.01	0.04	0.09	7.98	87.87
9550-5	5	0.03	0.09	0.48	0.43	2.78	5.52	0.01	70.83	0.06	0.08	3.37	83.68
Std. dev.		0.026	0.141	0.128	0.078	0.741	0.141	0.010	1.997	0.015	0.025	2.308	1.835
Average goethite													
Anal. #	*n*	Fe_2O_3	Al_2O_3	SiO_2	NiO	Cr_2O_3	TiO_2	MnO	CoO	SO_3	Total		
9550-1	5	68.38	6.69	na	0.22	2.05	0.13	nd	na	na	77.47		
9550-2	5	41.98	13.64	15.16	0.34	1.59	0.99	nd	nd	nd	73.70		
9550-3	5	56.83	9.29	11.78	0.64	2.14	0.19	3.51	0.85	0.1	85.33		
9550-4	5	34.57	15.99	11.39	0.99	1.49	0.33	2.53	0.28	nd	67.57		
9550-5	5	41.37	13.84	15.42	2.52	1.52	0.27	5.12	0.81	nd	80.87		
Std. dev.		13.71	3.79	2.15	0.93	0.31	0.35	1.31	0.32	–	6.79		

EPMA analytical conditions given in Online Resource F, Table F5

EDS analyses were done with a Camscan Microspec-4DV scanning electron microscope using a Link AN-1000 detector

na not analyzed; *nd* not detected

[a] 6, number analyses by EDS used in averages (except for NiO and CoO)

[b] 6, number analyses by EDS used in averages (except for NiO and CoO)

[c] 5, number analyses by EDS used in averages (except for NiO and CoO)

[d] 7, number analyses by EDS used in averages (except for NiO and CoO)

but in sample 9550-5, chromite comprises about 25 % of the sample. Chromite averages between 40 and 45 wt% Cr_2O_3, but some Cr/Al ratios may vary significantly leading to variation in backscatter intensity (average analyses given in Table 3). Different types of chromite occur, including particles showing vermiform alteration. X-ray photomicrographs of the goethite/halloysite mixture show finely intergrown particles with uniform distribution of Ni, local concentrations of Fe and Cr, and an area of high Al, which is gibbsite (Online Resource C, Fig. C4 a to g). SEM photomicrographs of some agglomerate particles in 9550-2 have Mn-rich areas together with some Ni (Online Resource C, Fig. C4h). Gibbsite (γ-$Al(OH)_3$) is an accessory phase in all samples. It occurs as separate masses, as rims between goethite and quartz and is probably mixed with halloysite in the matrix phase. Clinochlore [ideally $(Mg,Al)_6(Si,Al)_4O_{10}(OH)_8$] and talc (ideally $Mg_3Si_4O_{10}$) occur as isolated flakes or are intergrown in matrix material. They are more common in samples 9550-4 and 9550-5. These minerals invariably contain 15–20 wt% NiO, in addition to substantial amounts of Cr and occasional Ti (clinochlore only).

The results of the X-ray diffraction study of the "clay" mineral fractions after attrition milling are summarized in Online Resource F (Table F6), with the minerals listed approximately in order of abundance. It was noted after heating that sample 9550-2 shows 4.26 and 3.34 Å peaks, which may be ascribed to quartz. The chlorite mineral following heating collapses to about 12 Å in all the samples indicating a mixed-layer variety, possibly with smectite. An alternate possibility is that the sample contains vermiculite (formed by weathering) and it is an incomplete collapse to 10 Å. "Magnetite-Maghemite" represents a mineral within that group, maghemite being Fe-deficient magnetite ($Fe_{2.67}O_4$). "Garnierite" was used as a field term for core logging, but the actual Ni-bearing mineral(s) cannot be distinguished without EPMA. Green colors ascribed to "garnierite" would be masked by the dominant goethite indicated in Online Resource F (Table F6).

The hydroseparation concentrates consisted mostly of rounded to subhedral particles of chromite with minor resistate minerals zircon ($ZrSiO_4$), baddeleyite (ZrO_2), monazite $(REE)PO_4$, and thorianite (ThO_2), but with more variation between samples for the rare resistate primary minerals: arsenopyrite (FeAsS), ilmenite ($FeTiO_3$), pyrite (FeS_2), sphalerite (ZnS), galena (PbS), gersdorffite (NiAsS), rutile (TiO_2), ullmannite (NiSbS), and xenotime (YPO_4) and rare secondary minerals: altaite (PbTe), barite ($BaSO_4$), clausthalite (PbSe), smithsonite ($ZnCO_3$), and uraninite (UO_2) (Online Resource C, Table F7).

The weighted distribution of Au, Pd, and Pt between clay and grit after attrition milling shows that from 52 to ~59 % of the metals is present in the clay fraction (Cabri and Wilhelmij 2015). Assays show increasingly regular trends with regolith depth for the grit fraction, except for the deepest Au assay (Online Resource C, Fig. C5). The relative masses of precious metals calculated from minerals show similar trends for Pt and Au, but with a steeper trend for Au suggesting accumulation of secondary gold minerals (Online Resource C, Fig. C7). A total of 139 PGM, gold and silver minerals were found in the five samples, with a variable distribution across the profile as summarized in Table 4. Sperrylite is the major precious-metal mineral found (~50 %), followed by "electrum", isoferroplatinum, and gold. Other precious-metal minerals are found in trace quantities and include cabriite, platinum, tetra-auricupride, tetraferroplatinum, tulameenite, and five unidentified minerals (Online Resource E, Table E3). A selection of precious-metal minerals is shown in Online Resource C in Figs. C7 to C10. The grain-size distribution of the PGM and Au minerals is shown by relative weight percent (a) and by frequency (b) in Fig. 11 and mineral association data for the PGM are summarized in Fig. 12.

Discussion and conclusions

Primary mineralization

The primary samples come from impersistent stratiform layers or reefs of chromite and sulfide-rich harzburgite that contain

Table 4 Mineralogical distribution of precious metals with laterite regolith depth

Lithology and depth (m)	Sample	Primary minerals	Secondary minerals	Unstable primary minerals
Ferricrete: 2.4–5.0	9550-1	Pt-Fe alloy, rustenburgite	Native gold, cabriite?	Sperrylite, Pt and Pd tellurides, primary sulfides, electrum
Ferralite clay: 5.0–7.25	9550-2	Pt-Fe alloy, sperrylite	Native Pt, Native Au, native Ag, Pd_2Te, Pd-Ag-Se, tetra-auricupride	Pt and Pd tellurides, electrum, primary sulfides
Chromite saprolite: 7.25–9.5	9550-3	Pt-Fe alloy, sperrylite, electrum, acanthite?	Tetraferroplatinum	Pt and Pd tellurides, primary sulfides
Chromite saprolite: 9.5–14.0	9550-4	Pt-Fe alloy, sperrylite, electrum	Native Au, Pd alloy, Pd-bearing heazlewoodite, Pd-bearing millerite	Pt and Pd tellurides, primary sulfides
Chromite saprolite: 14.0–18.5	9550-5	Pt-Fe alloy, sperrylite, electrum, acanthite?, UK Pd_2NiSi	Native Au, Pd telluride, tulameenite	Pt and Pd tellurides, primary sulfides

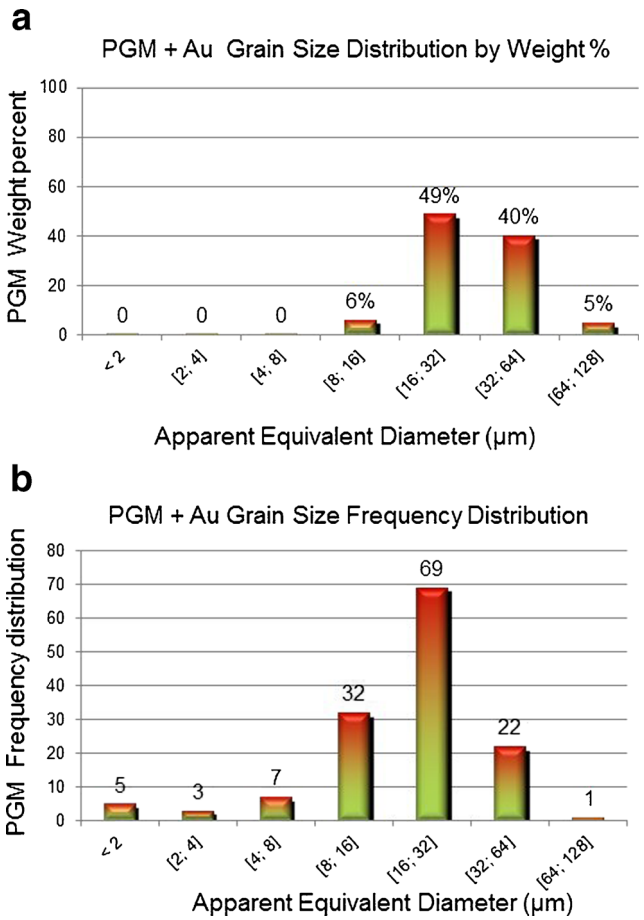

Fig. 11 PGM and Au minerals grain-size distribution by weight % (**a**) and frequency (**b**), regolith (n=134)

high-grade PGE mineralization (1–12 g/t 3E), and form part of the MCSS of the Lower Ultramafic Sequence that is well preserved in the Lubalisi Zone of the Kapalagulu Intrusion. In the Lubalisi Zone, the MCSS forms a syncline with the PGE reefs best developed in the northwestern limb of the fold. The folded MCSS is underlain by the Lower Feldspathic Harzburgite that contains little sulfide and chromite mineralization and overlain by the Sulfide Harzburgite that in places contains abundant thin chromite bands and widespread low-grade PGE mineralization. High-grade PGE mineralization is present in small massive differentiated sulfide and magnetite bodies that cut across the Lower Feldspathic Harzburgite sequence.

In the Lubalisi Zone, no significant PGE mineralization has been found in the Layered Troctolite and Harzburgite that marks the transition between the harzburgite of the Lower Ultramafic Sequence and the layered gabbro of the Upper Mafic Sequence of the Kapalagulu Intrusion. Low-grade PGE mineralization has also been found in sulfide- and chromite-rich layers in up to 100 m thick harzburgite that forms the base of the Makambo and Kapalagulu Zones of the Kapalagulu Intrusion (Maier et al. 2008; Wadsworth et al. 1982; Van Zyl 1959). However, it is likely that an unknown thickness of this basal harzburgite containing further PGE mineralization has been removed by faulting along the contact with the Ubendian gneiss. Although sulfide-bearing gabbroic rocks are present in the well-layered and exposed Upper Mafic Sequence, an extensive exploration effort failed to find any PGE reefs.

The PGE mineralization present in the approximately 1000 m-thick harzburgite sequence preserved in the Lubalisi Zone appears to represent the transition from low-sulfide mineralization, with the presence of PGE reefs, to high-sulfide mineralization, where there is widespread low-grade PGE mineralization associated with thick intervals of disseminated and net-textured sulfides (pyrrhotite, chalcopyrite and pentlandite) and PGE reefs are absent (Green and Peck 2005). The small massive sulfide bodies present in the Lower Feldspathic Harzburgite might represent coalesced sulfide melt derived from the overlying Sulfide Harzburgite that migrated downwards into their present stratigraphic position. No samples from the massive sulfide bodies in the Lower Feldspathic Harzburgite and the low PGE-grade Sulfide Harzburgite that overlies the MCSS were examined in our PGM mineralogical study.

The reef style of PGE mineralization in the MCSS harzburgite is reminiscent of the Merensky and UG2 Reefs of the Bushveld Complex rather than the Main Sulfide Zone of the Great Dyke in Zimbabwe or Main Sulfide Layer of the Munni Munni Complex in Western Australia which do not contain chromite enrichment (Barnes et al. 1992; Prendergast and

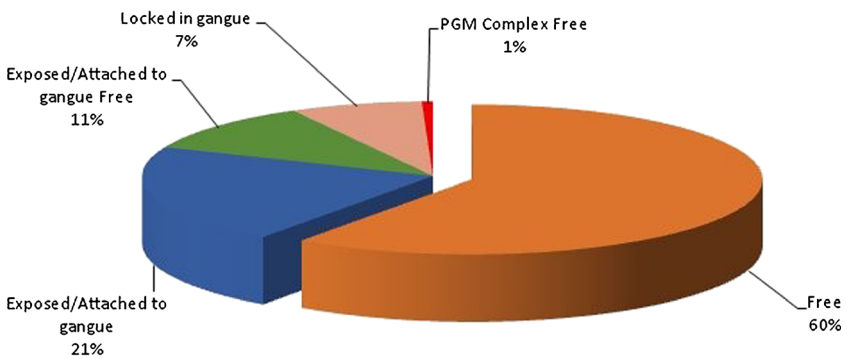

Fig. 12 Summary of association data for laterite regolith samples (KPD22), weight % (n=134)

Keays 1989; Wilson and Tredoux 1990; Kruger 2005). In the latter intrusions, the MSZ and Main Sulfide Layer (MSL) reefs are located in pyroxenite at the contact between lower ultramafic and upper mafic sequences. Unlike the MSZ and MSL, no vertical Pd and Pt offset style of mineralization (Prendergast 1988; Barnes et al. 1992) has been identified within individual PGE reefs of the MCSS, rather the PGE concentrations closely reflect the chromite and sulfide contents of the harzburgite host rock. It is possible that large-scale (thicknesses of tens of meters) Pd and Pt offset mineralization is present in the Sulfide Harzburgite that overlies the MCSS and this pattern of mineralization needs to be investigated by examining various precious and base metal ratios present in sampled drill core.

Within the western Bushveld Complex, the thin Merensky Reef and UG2 Chromitite Seam are located within the Critical Zone which represents the transitional zone between the ultramafic rocks of the Lower Zone and the gabbronorite of the Main Zone (Kruger 2005). It is clear that the stratigraphic location of the MCSS reefs within the Lower Ultramafic Sequence of the Lubalisi Zone is different to the Merensky and UG2 reefs of the Bushveld Complex and should rather be compared to the Lower Group (LG) of chromitite seams present in the ultramafic rocks of the Lower Zone (Maier 2005). However, the LG chromitite seams have been traced over hundreds of kilometers along strike and down-dip to depths of 2 km which contrasts to the PGE reefs of the MCSS which are impersistent and confined to a narrow dike-like body that is 2 km wide and deeper than 1000 m, largely filled by poorly stratified harzburgite and lesser dunite. These PGE reefs, like the Bushveld Complex PGE-bearing chromitite seams and (LG and UG2) and Merensky Reef, represent a low-sulfide style of magmatic PGE mineralization which contrasts with the extensive low-grade PGE mineralization present in the overlying Sulfide Harzburgite that represents high-sulfide magmatic mineralization. In the latter, the presence of abundant disseminated and net-textured sulfides and associated low-grade PGE mineralization over wide stratigraphic thicknesses implies that the PGE reefs are either very poorly defined or absent. There is a need to study the PGE mineralization of the Sulfide Harzburgite lithostratigraphic unit in more detail by reviewing geochemical data obtained from penetrating drill holes.

The modal distribution of the Pd minerals is quite different among the three primary samples from the MCSS that were fully studied mineralogically (Online Resource E, Tables E1 and E2; Cabri et al. 2015, Table 1): the dominant Pd minerals in D395 are bismuthides and bismuthtellurides, in D396 they are tellurides, followed by bismuthtellurides, and stannides, and for 10369 they are antimon-arsenides, stannides, and tellurides. Also to be noted is the difference between frequency and mass% where, for example, Pd alloys are twice as abundant as Pd stannides, but the reverse is true by relative mass%. On the other hand, the Pt minerals have similar modal distributions for the three samples: the dominant Pt minerals are arsenides (i.e., sperrylite) followed by tellurides. The contrast between mass% and frequency for these two mineral groups is quite pronounced, in that, for example, the Pt tellurides are most abundant in 10369 but are third in terms of mass%.

Comparison of Pd/Pt ratios from whole rock assays to those calculated from mineral data show that the mineral data for the Pt and Pd PGM are very robust (Table 5). Small samples are more likely to show variability in the calculated ratios, which may increase when using ideal densities for PGM, adding to the errors. The results confirm that the methodology used to concentrate and characterize the PGM was very successful and that the modal analyses of PGM are reliable for these samples. In contrast, ratios using Au compare poorly, most likely because gold concentrations in the samples are very low (0.14 to 0.18 ppm), but also because some Au may occur in solid solution in the BMS, and in rare particles of gudmundite and arsenopyrite. The latter minerals were found associated in one case with aurostibite in sample D396, which together are considered to represent later hydrothermal mineralization, and which can be related to the extensive sulfide remobilization and micro-veinlets seen in drill core.

Though samples D395 and D396 are contiguous, the PGM and gold minerals in the former are coarser-grained compared to those in sample 10369 (Online Resource E, Tables E1 and

Table 5 Pt, Pd, and Au ratios from assays compared to calculated ratios from minerals

Sample	Type	Pd/Pt	Pd/Au	Pt/Au	Pd+Pt/Au	Pd+Pt+Au/Pt
		Sulfide samples				
D395	Assay	0.4	54.3	22.9	77.2	3.4
	Minerals	0.5	0.1	33.9	52.1	1.6
D396	Assay	0.4	15.1	5.7	20.7	3.8
	Minerals	0.5	1.2	2.2	3.4	2.0
10369	Assay	0.7	21.9	14.9	36.8	2.5
	Minerals	0.7	1.1	1.5	2.6	2.4
81914	Assay	1.0	4.3	4.5	8.8	2.2
	Minerals	No HS done, only 11 PGM found				
		Laterite regolith samples				
9550-1	Assay	0.6	11.0	17.0	28.0	
	Minerals	0.1	0.1	0.6	0.7	
9550-2	Assay	1.0	4.3	4.2	8.5	
	Minerals	0.1	0.2	3.6	3.8	
9550-3	Assay	1.1	3.9	3.6	7.5	
	Minerals	0.0	0.0	0.9	0.9	
9550-4	Assay	1.2	3.1	2.6	5.7	
	minerals	0.0	0.0	1.0	1.0	
9550-5	Assay	1.0	7.1	6.8	14.0	
	Minerals	0.0	0.0	1.9	1.9	

E2; Cabri et al. 2015; Table 1). However, the samples are too small to further explore the significance of this aspect.

Samples D396 and 10369 show evidence of unusual conditions during crystallization, possibly involving very low fO_2 and fS_2. The presence of the new mineral palladosilicide, Pd_2Si (12 very small particles), which has an unusual composition, together with the occurrence of several relatively abundant alloy species in sample 10369 and the presence of troilite in sample D396 suggests conditions of low fS_2. The possible conditions for crystallization of this unusual new mineral are further discussed in Cabri et al. (2015).

Comparison of the precious-metal mineralogy of the sulfide-bearing samples at Kapalagulu to other major PGE deposits shows marked differences. At Kapalagulu sperrylite dominates, sobolevskite is important as are Au alloys, as well as antimonides and stannides. However, there are only trace Pt-Pd sulfides in contrast to, e.g., the importance of Pt-Pd sulfides in the Merensky reef (Schouwstra et al. 2000), MSZ (Coghill and Wilson 1993; Evans et al. 1994; Evans and Spratt 2000; Oberthür et al. 1997, 2013b), and J-M reef (Todd et al. 1982).

Oxidized mineralization

The laterite regolith (oxide) samples come from ferricrete, red saprolite clay, and chromite saprolite clay in which there is a progressive downward increase in PGE mineralization. This mineralization represents the surface expression of one of the PGE reefs present in the MCSS harzburgite that dips to the southwest in the northeastern limb of the Lubalisi Syncline.

In the laterite regolith of the Lubalisi Zone, there is a characteristic vertical geochemical pattern which consists of:

1. An upward increase in Fe_2O_3 content which peaks in the ferruginous red clay and ferricrete.
2. A dramatic upward decrease in the MgO content due to loss of magnesium from the protolith by chemical weathering processes.
3. An upward increase in the Al_2O_3 content due to the formation of aluminum-rich clays.
4. A concentration of Ni in the lower saprolite clay due to supergene enrichment.
5. A residual concentration of Cr in the upper saprolite clay that is partly associated with the zone of Fe_2O_3 concentration.
6. A concentration of PGE in the saprolite clay and associated saprock that reflects the residual nature of the PGE mineralization which is spatially related down-dip to inclined chromite-sulfide harzburgite layers that represent PGE reefs in the MCSS harzburgite.

Thus, in the Lubalisi laterite regolith the PGE concentrations appear to represent a combination of residual mechanical and supergene enrichment due to chemical weathering processes. As lateritization leads to the transfer of materials followed by variations of volume and density of the original rock various enrichment factors can be used to determine the amount of material transferred. To determine enrichment factors, a chemical reference element is needed, which is very immobile (such as Ti) and consequently has not been modified by lateritization fluids. The ratio between Al_2O_3 and Fe_2O_3 is another method that can be used to study residual enrichment in a laterite regolith (Bandyayera 1997). Laterite profiles from the Lubalisi plateau resemble those covering part of the Musongati Intrusion in eastern Burundi. Here, the laterite overlies a dunite and harzburgite protolith that is similar to that present in the Lubalisi Zone (Bandyayera 1997). In his study of the Musongati laterite, Bandyayera used petrography and geochemistry to identify the weathering processes that lead to the concentration of nickel and PGE. He concludes that the development of the laterite regolith profile is the result of long, severe and cyclic alteration processes of the ultramafic protolith under subtropical weathering conditions. Material movements were dominantly vertical and controlled by water-table fluctuations. Fluids responsible for recent lateritization follow the same path as earlier ones, or the path produced by older alteration events. The alteration front progresses through the regolith from the surface to the base of the saprock, and with time, each horizon of the laterite forms from the underlying horizon.

Pt/Pd ratios for pristine Kapalagulu samples range from 0.31:1 to 0.98:1 (Table 1). However, the average ratio for the MCSS harzburgite (including the PGE reefs from 3286 samples and 36 drill holes) that contained Pt and Pd above detection is 1.21:1. A different Pt/Pd ratio of 2.39:1 is obtained for the low-grade mineralization present in the overlying Sulfide Harzburgite sequence, which shows that there has been platinum enrichment compared to the MCSS. Thus, the average ratios from the MCSS are similar to the laterite regolith, which range from 1.52:1 at the surface (soil) to 1.33: in depth (saprock) for 1030 drill holes (as shown in Table F8 Online Resource F), but these are very different for the Sulfide Harzburgite. This implies that Pd is more mobile in the supergene environment than Pt, as was shown by Evans et al. (1994) and Oberthür et al. (2013b) for Great Dyke surface ores and pervasively oxidized MSZ at the Hartley mine, respectively. However, we are unable to confirm whether the residual and supergene PGE mineralization of the laterite regolith from which the samples for the PGM study came from had the same Pt/Pd ratio as the pristine samples.

Bandyayera (1997) considers that PGE concentrations in the lateritic horizons are strongly modified by supergene processes and that there are three to four times more PGE in the regolith compared to the protolith indicating residual enrichment. It appears that Au, Pd and Pt are mobile in all of the Musongati lateritic horizons with Au more mobile than Pd

which is in turn more mobile than Pt, Rh, Ir, and Ru, which are relatively immobile.

The assays of the clay and grit fractions for the five samples from the regolith (Online Resource, Table D2) were used to calculate a single weighted value for the core: Au 268, Pd 1388, and Pt 1253 (ppb); Ni 6448, Cu 2442, and Co 642 (ppm); 3.28 % Cr. However, comparing bulk assays for each sample in the grit fraction to those in the clay fraction with depth from the surface in the drill hole show different distributions for some elements. In general, the grit fractions show increased Au, Pd, Pt, Ni, and Cu from the surface down (Online Resource C, Figs. C12a). These trends are in contrast to the trends in the clay fraction (Online Resource C, Fig. C12b) where all metals show high to slightly higher values in the near-surface sample (9550-1, ferricrete laterite), evidence of accumulation and re-deposition, before a sharp to gentle drop in values in the underlying sample (9550-2, clay with some chromite). The metal values then increase in concentration with depth except for Ni that decreases in the deepest sample, as does Cu, but to a lesser degree. The combined weighted values for grit and clay fractions show features of both trends (Online Resource C, Fig. C12c). Examination of the weighted assay data for Au, Pt, Pd, and Ni shows that these metals dominate in the clay fractions of samples 9550-1, 9550-3, and 9550-5. In contrast, these metals dominate in the grit fraction of sample 9550-2 and Pt and Ni are dominant in the clay fraction of sample 9550-4 and Au and Pd dominate the grit fraction. Much more detailed study is needed to understand all the mineralogical implications but the dominance of metals in grit in sample 9550-2 is reflected by a corresponding sharp decrease in the metal contents for the clay fraction (Online Resource C, Fig. C12b).

The primary Pd mineralization, if it was similar to the described sulfide-bearing primary samples, has not survived oxidation as otherwise numerous Pd minerals would have been found in the HS concentrates. It is valid to inquire whether the methodology used here was the best for this type of sample.

In our samples, the Pd minerals and the Pd in solid solution in pentlandite are thought to have been mostly dissipated but some were reconstituted to form secondary minerals. Wagner (1929) describes oxidized Merensky Horizon to contain in part crystals of cooperite or sperrylite and partly minute colloform and nuggety grains ascribed by Schneiderhöhn (in Wagner 1929, p. 242) to represent "platinum metals that were originally in solution in magmatic sulphides." These intuitively correct observations were made long before microanalytical techniques could be used and when few PGM were known, but to the authors' knowledge the nature of these colloform grains has not been examined. Oberthür et al. (2013b) reported that platinum-iron alloy grains are either compact idiomorphic cubic crystals, or they occur as porous grains in samples of oxidized MSZ (Zimbabwe). They write "The porous grains of Pt-Fe alloy (close to Pt_3Fe in composition) probably represent replacements of other precursor PGMs of unknown chemical composition (see Fig. 7f)". Notably, Schneiderhöhn and Moritz (1939) showed texturally similar porous grains of "native Pt" from oxidized Merensky Reef and proposed that these grains represent relicts of sperrylite or cooperite grains. Graphic intergrowths of Pt-Fe alloys (both isoferroplatinum and tetraferroplatinum) with BMS and magnetite were reported from unoxidized Merensky Reef (Cabri et al. 2008) and from the River Valley intrusion of the Sudbury area (Cabri 2002, Fig. 40-2). It is therefore likely that the alloys studied by Schneiderhöhn and Moritz (their Plate 3) represent resistate Pt-Fe alloys after oxidation of primary BMS.

Only six Pd PGM were found in the grit fractions (cabriite, unnamed tellurides, a selenide, and alloys) in the two uppermost layers and potentially Pd-bearing secondary sulfides (millerite and heazlewoodite) and a Pd-Te-Hg mineral in the two lowest layers. Comparison of the distribution of Pd mineral species to those in the primary ore is shown in Fig. 13. The primary Pt minerals are more resistant to oxidation and dissolution, especially Pt-Fe alloy (isoferroplatinum) and

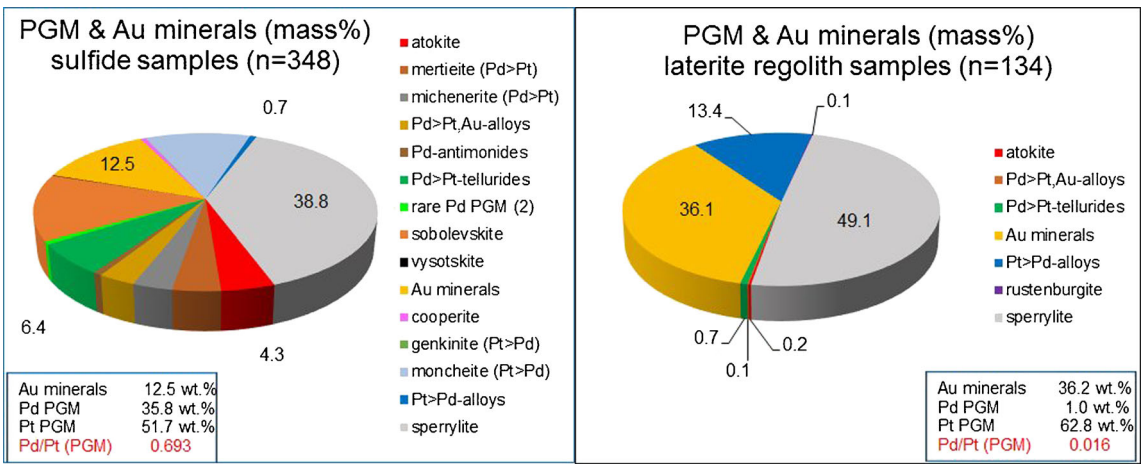

Fig. 13 Comparison of PGM and Au-Ag minerals found in sulfide samples with those in the laterite regolith by mass%

sperrylite, but it is likely that other Pt alloys are of secondary origin (from dissolution of Pt tellurides) limiting the Pt PGM species to two main types: arsenide (sperrylite) and alloys as can be seen by comparison to Pt species in the primary mineralization (Online Resource E, Tables E1 and E2; Cabri et al. 2015; Table 1). Whereas mineralogical data are scarce for the upper two samples, compared to the lower three, the average ECD of the precious metal minerals is very similar for the two groups, being 21.1 and 21.6 μm, respectively. However, the lower group samples have a broader size-range, up to an ECD of 67 μm.

The Pt/Au ratios from assays compared to those calculated from minerals only correspond fairly closely for sample 9550-2 (4.2 vs. 3.6) as shown in Table 5. This is the only sample which has a slightly greater proportion of metals in the "grit" fraction than in clay, as noted above. The shallowest sample (9550-1) shows the greatest divergence and lowest metal values, containing only 38 ppb Au, so that the poor correlations may be mostly due to statistics.

Wagner (1929, p. 110) gives assays for sulfide and oxidized ores in Rustenburg and Lydenburg, concluding that "The ratio of platinum to palladium is from 7 to 10 per cent. higher in the oxidized zone than in the sulphide zone, the palladium being clearly more susceptible to leaching by oxygenated surface waters." On p. 250, Wagner describes a concentrate from oxidized "reef" at the Wedza Platinum Mine (Great Dyke) that contains Pt mainly in the form of sperrylite and cooperite. Cabri and Chen (1976) reported examining 36 slices of a deeply weathered sample from Farm Tweefontein (16 miles from Potgietersrust, South Africa) where the only metallic minerals found were sperrylite and pyrite. The susceptibility of most primary Pd minerals to weathering has been shown in numerous other studies especially on the Great Dyke (e.g., Evans et al. 1994; Evans and Spratt 2000; Oberthür et al. 1999, 2000, 2003, 2013a, b; Prendergast 1990), and on the UG2 chromitite (Hey 1999), and references therein.

The major PGE reefs in the Bushveld, the MSZ in Zimbabwe, and the J-M reef in Montana contain Pt and Pd PGM, as well as variable but important concentrations of Pd in pentlandite. Among the first reports of solid solution Pd in pentlandite are Todd et al. (1982) in the J-M reef, Cabri (1988) in Merensky reef samples, and Oberthür et al. (1997) in the MSZ. Pentlandite, together with other sulfides, breaks down during weathering forming various secondary minerals in oxidation zones.

Detailed work done at BGR (Bundesanstalt für Geowissenschaften und Rohstoffe) on the oxidized MSZ and stream sediment samples, as summarized in Oberthür et al. (2013b) found that "Within the oxidized MSZ ores, the PGE are polymodally distributed. Whereas the arsenide- and sulfide-PGMs that make up approximately 25 per cent of the original Pt content of the ore largely remain stable (form relict PGMs), the remaining PGMs are disintegrated. The base metal sulphides are destroyed, partly releasing their base metal and PGE contents, and are replaced by iron oxides or hydroxides. Unspecified amounts of the PGE are redistributed and either form secondary PGMs, are found in chemically and mineralogically ill-defined (Pt/Pd)-oxides or hydroxides, or in iron-hydroxides, Mn–Co-hydroxides, and in secondary silicates."

As summarized above, the apparent loss and dispersal of Pd compared to Pt has been widely reported but is not evident from our assays of the laterite regolith samples taken from a single drill hole in saprock so that it is difficult to make larger-scale conclusions regarding this laterite weathering process. There is a need to take into account the different amounts and ratios of Pt and Pd that are present in the MCSS and overlying Sulfide Harzburgite protolith. In bore hole KPD22 Pt, Pd, and Cr have similar trends, as well as Au (but less well), and Ni and Ni/Cu show the usual concentrations in the saprock and overlying saprolite below the PGE-rich horizons (Online Resource A, Fig. A5). However, the saprolite clays represent a very different weathering environment to the saprock in that the former underwent Mg loss. On the other hand, assay ratios derived for a large database for different lithologies at Kapalagulu show that there is a progressive increase in Pd and Au ratios relative to Pt with depth in the laterite profile indicating Pd and Au loss relative to Pt in the near-surface laterite lithological units (Online Resource F, Table F8).

Thus, there is no directly applicable comparison between the precious-metal minerals found in the regolith to those reported by Evans et al. (1994), Evans and Spratt (2000), and Oberthür et al. (2013b) on weathered MSZ (and stream sediment samples), as well as by Becker et al. (2014) on weathered Bushveld "silicate reef". The relative paucity of Pd minerals found in the laterite regolith samples, and their fine-grained nature, further suggests that other than the occurrence of some secondary Pd minerals, all the primary Pd mineralization has been dissipated or reconstituted, albeit without precise knowledge of the sulfides and PGM in the precursor mineralized harzburgite. Some of the dispersed Pd may occur in remnant secondary minerals such as heazlewoodite and millerite, both known to be Pd-carriers. It is also obvious that the Pd formerly in solid solution in pentlandite has now been redistributed and dispersed, some of which may be retained as a physical mixture in the goethite that has replaced the sulfide minerals.

Some of the primary Pt minerals occurring at Kapalagulu are known to be more resistant to oxidation and dissolution, such as Pt-Fe alloy (isoferroplatinum) and sperrylite, but it is likely that native platinum, tetraferroplatinum, and tulameenite are of secondary origin since they are not found or are sparse in the primary sulfide samples and have been

reported to be secondary minerals elsewhere. For example, tetraferroplatinum partially replaces isoferroplatinum in the rim of a nugget from Ethiopia (Cabri et al. 1981) and Zhernovskiy et al. (1985) report from Russian deposits similar but narrower rims of tetraferroplatinum, as well as tulameenite occurring in rims and exsolution textures.

Unpublished research at BGR, Hannover, on three different regolith samples (each sample being a composite of an individual laterite horizon) found two Pt-Fe alloy particles in one concentrate and a single particle of an Fe-Al hydroxide with gold crystals in another concentrate (Fig. 14). It appears that the crystalline nature of the Pt-Fe grains is similar to primary isoferroplatinum crystals from Stillwater (e.g., Cabri 1981; Figs. 7.22A and 22B) suggesting that they represent primary mineralization. The absence of sperrylite in the uppermost sample (9550-1) may be a nugget effect due to relatively lower Pt grade, whereas other primary PGM such as moncheite are no longer stable and their Pt content is now dispersed. Some of the Pt and Pd derived from altered PGM and from solid solution in sulfides may have remained as friable grains intergrown with secondary Fe-oxide minerals but were lost during hydroseparation. Because sperrylite is so stable, it is possible that it is still present in sample 9550-1, but in the form of very fine unrecovered particles, though there were no signs of alteration on the sperrylite particles found. However, sperrylite is known to slime easily and tends to break down to finer-grained particles even when locked in goethite. Regardless, the poorer correlation between assay and mineralogy (Online Resource C, Fig. C6) for the uppermost sample (yellow-brown ferricrete laterite) suggests that some Pt is not accounted for in the mineralogy. Like Pd, one cannot be certain of the present location of the dispersed Pt, but it is likely to also be physically associated with goethite, as well as with Mn-wad.

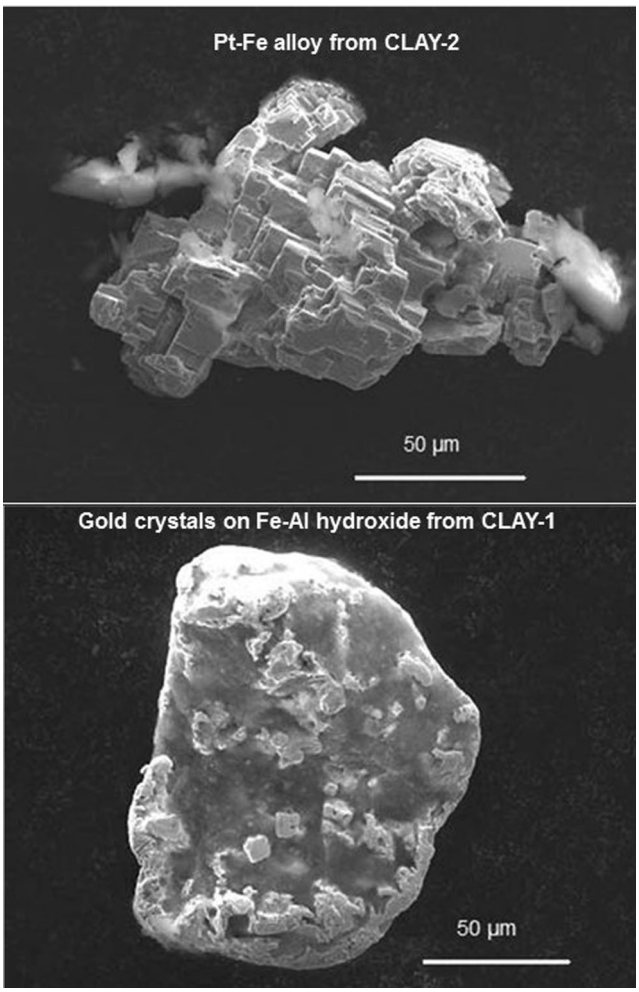

Fig. 14 SEM images of Pt-Fe alloy and gold on Fe-Al hydroxide aggregate in concentrates (Oberthür 2004, unpublished)

No Pt or Pd "oxides" were found in this study nor reported in the study of oxidized "silicate reef" by Becker et al. (2014), in contrast to the reports from the Great Dyke (Zimbabwe) by Evans (2002) and Oberthür et al. (2003). Most of the latter and related papers describe Pt and Pd oxide/hydroxide "minerals" that are controversial as none have been sufficiently characterized to be officially recognized as discrete bona-fide minerals. Recent research into this type of mineralization from New Caledonia used X-ray absorption to study Pt and Fe in O-bearing Pt-Fe grains (Hattori et al. 2010). They concluded that the O-bearing Pt-Fe is a physical mixture of relict isoferroplatinum and newly precipitated Fe^{3+}-O-OH, suggesting that O-bearing Pt-Fe mixture formed by the dissolution of Fe^0 followed by the dissolution of Pt^0 from isoferroplatinum and precipitation of Fe^{3+} during weathering of host ultramafic rocks. Similarly, Zaccarini et al. (2014) examined Ru-rich grains in chromitite associated with the altered harzburgite from Loma Peguera (Dominican Republic). They concluded that previously described Ru oxides consist of a fine-grained intergrowth of ruthenium and magnetite not detectable at the scale of the electron microprobe. A detailed high-resolution micro-analytical study of Pt-Fe alloys from the semi-arid Fifield Au-Pt ferruginous paleochannel (New South Wales, Australia) by Brugger et al. (2013) reports that isoferroplatinum grains showed no signs of supergene reprecipitation in contrast to gold grains, where secondary gold occurs as a dusting of pure metallic Au particles from <10 nm to >10 µm in diameter.

Gold that originally occurred as "electrum" has in some cases been leached of Ag, resulting in relatively pure native gold in all five samples, sometimes occurring together with "electrum", as well as forming native silver. A small proportion of the Au has also been recrystallized to form secondary tetra-auricupride, which was found in sample 9550-2.

Silver, originally occurring in "electrum" and in some Ag sulfides and Ag tellurides, has recrystallized in the form of native silver in sample 9550-2. Some of the Ag has

recrystallized as a Pd-Ni-Ag alloy in sample 9550-4 and some may be dispersed in some of the gangue minerals.

The relative loss of Pt in the form of PGM to that of Au may be shown approximately by determining the Pt/Au ratio in the present samples from assay values for "grit" (Table 5) compared to the ratio determined from the mass weights of Pt and Au determined from the measured Pt and Au minerals. Whereas the numbers are not very precise, they support greater loss of Pt minerals with respect to Au minerals at variable depths (Online Resource C, Fig. C11). However, this trend may be masked and distorted by the tendency of gold minerals to dissolve and reprecipitate.

Nickel does not form discrete minerals, with the exception of single particles of millerite (NiS) and a Pd-bearing heazlewoodite (and rare ullmannite and gersdorffite), but occurs in other minerals. It occurs in trace amounts in goethite, hematite, and chromite and about 15–20 wt% NiO occurs in clinochlore and talc. The most significant Ni carriers in the regolith samples are clinochlore and talc (85.0–97.7 %), even though they represent less than 2.5 % by abundance of the Ni carriers. The Ni contribution from goethite shows a slight progressive increase with depth, having been formed by oxidation of pentlandite, and Ni dispersal is mirrored by the progressive decrease in the Ni contribution from clinochlore and talc with depth (Table 5). The Ni distribution for hematite is erratic (0.5–2.6 %) and shows no progression and that for chromite shows a small range from 0.5 to 0.9 %, which is probably within experimental error.

Acknowledgments We are grateful for permission to publish by the joint venture partners (Lonmin PLC and Goldstream Mining NL), to Martine Wilhelmij for the maps and diagrams, to Martin Prendergast for his geology map of the Kapalagulu Zone and extensive discussions, to Thomas Oberthür for access to his unpublished data on PGM in oxidized samples and discussions, as well as discussions with Daniel Bandyayera and Thomas Aiglsperger on laterites. Wolfgang Maier provided his original map of the Central African Nickel Belt that was modified by Martine Wilhelmij. We also acknowledge the careful work done in different laboratories on behalf of Cabri Consulting Inc: Al Miller (Kishar Research Inc.) for petrography of PTS, Jeanne B. Percival (Geological Survey of Canada) for clay XRD, Rolando Lastra (Canmet) for image analysis, and Nikolay V. Rudashevsky (Center for New Technology) for screening, hydroseparation, and SEM analyses and images. The manuscript has been considerably improved by detailed comments and suggestions made by the referees (Martin Prendergast and anonymous), as well as by helpful suggestions by associate editor Wolfgang Maier and Editor Bernd Lehmann.

References

Almohandis AA (1984) Occurrence and the compositional variations of chromite in the Kapalagulu Intrusion, western Tanzania. Bull Faculty Earth Sci King Abdulaziz Univ 6:619–632

Bandyayera D (1997) Formation de laterites nickelifères et mode de distribution des éléments du groupe du platine dans les profils lateritiques du complexe de Musongati, Burundi. PhD thesis (unpubl.), Université du Québec à Chicoutimi, 440 pp

Barnes SJ, Keays RR, Hoatson DM (1992) Distribution of sulphides and PGE within the porphyritic websterite zone of the Munni Munni complex, Western Australia. Austr J Earth Sci 39:89–302

Becker M, Wiese J, Ramonotsi M (2014) Investigation into the mineralogy and flotation performance of oxidised PGM ore. Miner Eng 65:24–32

Boniface N (2009) Eburnian, Kibaran and Pan-African metamorphic events in the Ubendian belt of Tanzania: Petrology, zircon and monazite geochronology. PhD thesis, University of Kiel, 111pp

Boniface N, Schenk V (2012) Neoproterozoic eclogites in the Paleoproterozoic Ubendian Belt of Tanzania: evidence for a Pan-African suture between the Bangweulu Block and the Tanzania Craton. Precambrian Res 208–211:72–89

Boniface N, Schenk V, Appel P (2012) Paleoproterozoic eclogites of MORB-type chemistry and three Proterozoic orogenic cycles in the Ubendian Belt (Tanzania): evidence from monazite and zircon geochronology, and geochemistry. Precambrian Res 192–195:16–33

Brugger J, Etschmann B, Grosse C, Plumridge C, Kaminski J, Paterson D, Shar SS, Ta C, Howard DL, de Jonge MD, Ball AS, Reith F (2013) Can biological toxicity drive the contrasting behavior of platinum and gold in surface environments? Chem Geol 343:99–110

Cabri LJ (1981) The Platinum-Group Minerals, in Platinum-Group elements: Mineralogy, Geology, Recovery, Editor and principal contributor, CIM Special Volume 23, 267 pp. 2nd edition reprinted 1989, pp. 114

Cabri LJ (1988) Applications of proton and nuclear microprobes in ore deposit mineralogy and metallurgy. Nucl Instr Methods Phys Res B30:459–465

Cabri LJ (2002) The platinum-group minerals. In The Geology, Geochemistry, Mineralogy, Mineral Beneficiation of the Platinum-Group Elements. Ed. L.J. Cabri. Canadian Institute Mining, Metallurgy and Petroleum, Special Volume 54, 116-117

Cabri LJ, Chen TT (1976) Stibiopalladinite from the type locality. Am Mineral 6:1249–1254

Cabri LJ, Wilhelmij HR (2015) Contrasting mineralogical potential of two mineralization types in the precious metal and Ni-bearing Kapalagulu intrusion, western Tanzania. Minerals Engin (in preparation)

Cabri LJ, Criddle AJ, Laflamme JHG, Bearne GS, Harris DC (1981) Mineralogical study of complex Pt-Fe nuggets from Ethiopia. Bull Mineral 104:508–525

Cabri LJ, Beattie M, Rudashevsky NS, Rudashevsky VN (2005) Process mineralogy of Au, Pd and Pt ores from the Skaergaard Intrusion, Greenland, using new technology. Minerals Eng 18:887–897

Cabri LJ, Rudashevsky NS, Rudashevsky VN (2008) Current approaches for the process mineralogy of platinum-group element ores and tailings. Ninth International Congress for Applied Mineralogy ICAM 2008. Austral Inst Mining Metall, Public Ser No 8/2008: 9-17

Cabri LJ, McDonald AM, Stanley CJ, Rudashevsky NS, Poirier G, Wilhelmij HR, Zue W, Rudashevsky VN (2015) Palladosilicide, Pd_2Si, a new mineral from the Kapalagulu Intrusion, western Tanzania and the Bushveld Complex, South Africa. Mineral Mag 79(2):295–307

Coghill BM, Wilson AH (1993) Platinum-group minerals in the Selukwe subchamber, Great Dyke, Zimbabwe: implications for PGE collection mechanisms and post-formational redistribution. Mineral Mag 57:613–633

Deblond A, Punzalan LE, Boven A, Tack L (2001) The Malagarazi Supergroup of southeast Burundi and its correlative Bukoba Supergroup of northwest Tanzania: Neo- and Mesoproterozoic chronostratigraphy constraints from Ar-Ar ages on mafic rocks. J Afr Earth Sci 32:435–449

Duchesne J-C, Liégeois J-P, Deblond A, Tack L (2004) Petrogenesis of the Kabanga–Musongati layered mafic–ultramafic intrusions in

Burundi (Kibaran Belt): geochemical, Sr–Nd isotopic constraints and Cr–Ni behaviour. J Afr Earth Sci 39:133–145

Evans DM (2002) Potential for bulk mining of oxidized platinum-group element deposits. Trans Inst Min and Metall 111:B81–B86

Evans DM, Spratt, J (2000) Platinum and palladium oxides/hydroxides from the Great Dyke, Zimbabwe, and thoughts on their stability and possible extraction. Applied Mineralogy. Rammlmair et al. (eds.) AA Balkema, Rotterdam, 289-292

Evans DM, Buchanan DL, Hall GEM (1994) Dispersion of platinum, palladium and gold from the Main Sulfide Zone, Great Dyke, Zimbabwe. Trans Inst Min Metall 103:B57–B67

Green T, Peck D (2005) Platinum group element exploration: economic considerations and geological criteria. Mineralogical Association of Canada Short Course 35, Oulu, pp 247–274

Hattori K, Takahashi Y, Augé T (2010) Mineralogy and origin of oxygen-bearing platinum-iron grains based on an X-ray absorption spectroscopy study. Am Mineral 95:622–630

Hey PJ (1999) The effects of weathering on UG-2 chromitite reef of the Bushveld complex, with special reference to the platinum-group minerals. S Afr J Geol 102:251–260

Kraut JC, Stern WB (2000) The density of gold-silver-copper alloys and its calculation from the chemical composition. Gold Bull 33(2):52–55

Kruger FJ (2005) Filling the Bushveld Complex magma chamber: lateral expansion, roof and floor interaction, magmatic unconformities, and the formation of giant chromitite. PGE and Ti-V-magnetite Dep: Miner Dep 40:451–472

Lastra R, Wilson JMD, Cabri LJ (1999) Automated gold search and applications in process mineralogy. Trans Inst Min Metall Sect C 108:C75–C84

Maier WD (2005) Platinum-group element (PGE) deposits and occurrences: mineralization styles, genetic concepts, and exploration criteria. Invited presidential review. J Afr Earth Sci 41:165–191

Maier WD, Peltonen P, Livesey T (2007) The ages of the Kabanga North and Kapalagulu intrusions in western Tanzania: a reconnaissance study. Econ Geol 102:147–154

Maier WD, Barnes S-J, Bandyayera D, Livesey T, Li C, Ripley E (2008) Early Kibaran rift-related mafic–ultramafic magmatism in western Tanzania and Burundi: Petrogenesis and ore potential of the Kapalagulu and Musongati layered intrusions. Lithos 101:24–53

Oberthür T, Cabri LJ, Weiser TW, McMahon G, Müller P (1997) Pt, Pd and other trace elements in sulfides of the Main Sulfide Zone, Great Dyke, Zimbabwe. Can Miner 35:597–609

Oberthür T, Weiser TW, Gast L (1999) Mobility of PGE and PGM in the secondary environment at Hartley Mine, Great Dyke, Zimbabwe—a case study. In: Stanley CJ et al (eds) Mineral deposits: processes to processing. AA Balkema, Rotterdam, pp 763–766

Oberthür T, Weiser TW, Gast L, Wittich C, Kojonen K (2000) In: Rammlmair D et al (eds) Mineralogy applied to the evaluation and processing of platinum ores of the Main Sulfide Zone, Great Dyke, Zimbabwe. Applied Mineralogy, AA Balkema, Rotterdam, pp 379–382

Oberthür T, Weiser TW, Gast L (2003) Geochemistry and mineralogy of the platinum-group elements at Hartley Platinum Mine, Zimbabwe. Part 2: Secondary redistribution in the oxidized Main Sulfide Zone of the Great Dyke, and alluvial platinum-group minerals. Mineral Deposita 8:344–355

Oberthür T, Melcher F, Buchholz P, Locmelis M (2013a) The oxidized ores of the Main Sulfide Zone, Great Dyke, Zimbabwe: turning resources into minable reserves–mineralogy is the key. J. Southern Afr Inst Min Metall 113:191–201

Oberthür T, Weiser TW, Melcher F, Gast L, Wöhrl C (2013b) Detrital platinum-group minerals in rivers draining the Great Dyke, Zimbabwe. Can Mineral 51:197–222

Prendergast MD (1988) The geology and economic potential of the PGE-rich Main Sulfide Zone of the Great Dyke, Zimbabwe. In: Prichard et al. (eds) Geoplatinum 87, Elsevier pp. 281–302

Prendergast MD (1990) Platinum-group minerals and hydrosilicate 'alteration' in Wedza-Mimosa platinum deposit, Great Dyke, Zimbabwe – genetic and metallurgical implications. Trans Inst Min Metall (Sect B: Appl earth sci) 99:B91–B105

Prendergast MD, Keays RR (1989) Controls of platinum group element mineralization and the origin of the PGE-rich Main Sulphide zone of the Great Dyke, Zimbabwe: Implications for the genesis of, and exploration for stratiform PGE mineralization in layered intrusions, *in* Prendergast MD and Jones MJ, eds., Magmatic sulphides—the Zimbabwe volume: London, Inst Mining Metall: 43-69

Rabatho JP, Tongamp W, Shibayama A, Takasaki Y, Nitta S, Tetsuo Imai T (2011) Investigation of a flotation process with de-sliming and attrition to upgrade and recover Cu and Mo from a Cu-Mo flotation tailing. Mater Trans 52(4):746–752

Schneiderhöhn H, Moritz H (1939) Die Oxydationszone im platinführenden Sulfidpyroxenit (Merensky-Reef) des Bushvelds in Transvaal. Zentralblatt Mineralogie Geologie Paläontologie, Abteilung A, p 1–12

Schouwstra RP, Kinloch ED, Lee CA (2000) A short geological review of the Bushveld Complex. Plat Metals Rev 44(1):33–39

Tack L (1995) The Neoproterozoic Malagarazi Supergroup of SE Burundi and its equivalent Bukoban System in NW Tanzania: A current review. Royal Museum of Central Africa (Belgium). Ann Sc Geol 101:121–129

Todd SG, Keith DW, Le Roy LW, Schissel DJ, Mann EL, Irvine TN (1982) The J-M platinum-palladium reef of the Stillwater Complex, Montana. I. Stratigraphy and petrology. Econ Geol 77: 1454–1480

Van Zyl C (1956) The Kapalagulu Basic Complex, Tanganyika Territory. Unpubl. MSc thesis, Univ Pretoria, 74 pp

Van Zyl C (1959) An outline of the geology of the Kapalagulu layered complex, Kungwe Bay, Tanganyika Territory, and aspects of the evolution of layering on basic intrusives. Trans Geol Soc S Afr LXII: 1-31 (plus two Plates)

Vymazalová A, Laufek F, Kristavchuk AV, Chareev DA, Drábek M (2015) The system Ag-Pd-Te: phase relations and mineral assemblages. Mineral Mag 79: (in press)

Wadsworth WJ, Dunham AC, Almohandis AA (1982) Cryptic variation in the Kapalagulu Layered Intrusion, western Tanzania. Mineral Mag 45:227–236

Wagner PA (1929) The platinum deposits and mines of South Africa (Cape Town: C. Struik, 1929, reprinted 1973), 338 pp

Wilhelmij HR, Joseph G (2004) Stratigraphic location of platinum mineralisation in the Kapalagulu Intrusion of western Tanzania. Geosci Afr (Ed LD Ashwal) 2:709–708

Wilson AH, Tredoux M (1990) Lateral and vertical distribution of platinum-group elements and petrogenic controls on the sulfide mineralization in the P1 pyroxenite layer of the Darwendale subchamber of the Great Dyke, Zimbabwe. Econ Geol 85: 556–584

Zaccarini F, Bindi L, Garuti G, Proenza JA (2014) Ruthenium and magnetite intergrowths from the Loma Peguera chromitite, Dominican Republic, and relevance to the debate over the existence of platinum-group element oxides and hydroxides. Can Mineral 52: 617–624

Zhernovskiy IV, Mochalov AG, Rudashevskiy NS (1985) Phase inhomogeneity of iron-rich isoferroplatinum. Translated from: Fazovaya neodnorodnost' izoferroplatiny, bogatoy zhelezom. Doklady Akademi Nauk SSSR 283(1):196–200